TEM Examination of Advanced Alloys Irradiated in ATR

Jian Gan
Bruce A. Hilton

September 2007

INL
Idaho National Laboratory

TEM Examination of Advanced Alloys Irradiated in ATR

Jian Gan
Bruce A. Hilton

GNEP PIE Program Manager
Bruce A. Hilton

September 2007

Idaho National Laboratory
Nuclear Fuels and Materials Division
Idaho Falls, Idaho 83415

CONTENTS

FIGURES

TABLES

TEM Examination of Advanced Alloys Irradiated in ATR

1. INTRODUCTION

Successful development of materials is critical to the deployment of advanced nuclear power systems. Irradiation studies of candidate materials play a vital role for better understanding materials performance under various irradiation environments of advanced system designs. In many cases, new classes of materials have to be investigated to meet the requirements of these advanced systems. For applications in the temperature range of 500-800ºC which is relevant to the fast neutron spectrum burner reactors for the Global Nuclear Energy Partnership (GNEP) program, oxide dispersion strengthened (ODS) and ferritic-martensitic steels (e.g., MA957 and others) are candidates for advanced cladding materials. In the low temperature regions of the core (<600ºC), alloy 800H, HCM12A (also called T-122) and HT-9 have been considered.

The work summarized in this report focuses on microstructural characterization of four advanced alloys: nickel-based MA754 (ODS) alloys, iron-based HCM12A and MA957 (ODS) ferritic alloys, and high Ni austenitic alloy 800H, irradiated with neutrons to relatively low dose (1.1~1.5 displacements per atom [dpa]) at 500°C and 800°C in the Advanced Test Reactor (ATR) at the Idaho National Laboratory (INL). The irradiation conditions are listed in Table 1. The variation in the irradiation dose is due to the axial position of the test specimens and the flux variation in the axial direction. The temperature control was based on gamma heating of the specimens and heat transfer through an argon and helium gas mixture in the specimen capsule with the target temperatures of 500°C and 800°C. No in-line temperature measurement was conducted, so temperature was determined by analysis. Alloy composition is listed in Table 2.

Table 1. Summary of the irradiation experiment.

Alloys	Irradiation Temperature (C°)	Days of Irradiation (EFPD)	Neutron fluence (E>1 MeV) (neutrons/cm^2) (dose in dpa)
HCM12A	500	110.8	7.8 x 10^{20}, (1.1 dpa)
MA754	500	110.8	8.2 x 10^{20}, (1.2 dpa)
MA957	500	110.8	8.5 x 10^{20}, (1.2 dpa)
800H	500	110.8	8.8 x 10^{20}, (1.3 dpa)
MA957	800	110.8	9.9 x 10^{20}, (1.4 dpa)
800H	800	110.8	10.2 x 10^{20}, (1.5 dpa)
			Use 7x10^{20} n/cm^2 = 1.0 dpa for dpa calc.(Ref.)

Table 2. Chemical compositions of the alloys investigated.

Alloys	Density g/cm^3	Si	Ti	Al	C	N	Fe	Ni	Cr	W	Other element
HCM12A	8.03	0.26	--	--	0.11	0.07	Bal.	--	11.28	1.83	1.03Cu, 0.67Mn 0.39Ni, 0.007B
MA754	8.3	--	0.5	0.3	0.05	--	1.00	78	20	--	0.6Y$_2$O$_3$
MA957	7.8	0.04	1.05	0.10	--	--	84.13	0.13	13.87	--	0.30Mo, 0.08Mn 0.25Y$_2$O$_3$, ~0.17O
800H	7.94	0.13	0.57	0.50	0.069	--	45.26	31.59	20.42	--	0.76Mn

After irradiation, the capsules of disc samples (3 mm diameter and ~200 μm thickness) were transferred to the Hot Fuel Examination Facility (HFEF) at the Materials and Fuels Complex (MFC) for transmission electron microscopy (TEM) disc retrieval. The irradiated TEM discs were then transferred to the Electron Microscopy Laboratory (EML) at MFC for TEM sample preparation and microstructural characterization. For austenitic alloys (800H and MA754), the 3.0 mm diameter TEM discs were ground down to ~150 μm. For ferritic stainless steels (MA957 and HCM12A), a smaller disc format (2.3 mm diameter and ~70 μm thickness) was used to minimize the magnetic interference with electron beams during TEM analysis. TEM discs were electro-chemical jet polished to perforation using 5% perchloric acid in methanol at a temperature of approximately −40°C. A JEOL 2010 transmission electron microscope with LaB$_6$ filament and a Gatan UltraScan1000 digital camera was used for characterization.

2. TEM ANALYSIS OF IRRADIATED ADVANCED ALLOYS

The microstructural analysis consists of characterizing the radiation-induced microstuctural features such as cavities, loops, precipitates, and dislocations. In addition, for ODS alloys, the changes in oxide particle size distribution and number density are estimated. The effect of radiation on oxide particle stability is evaluated. Results of the microstructural analysis from the unirradiated alloys of the same batch are used for comparison with the results of the irradiated alloys. In the following sections, the analysis for each irradiated alloy, 800H, MA754, MA957 and HCM12A, will be presented first and then compared with its unirradiated condition. Due to the saturation of Energy Dispersive Spectrometer (EDS) detector from the radiation of the irradiated TEM specimens, composition analysis for precipitates is only available for the sample with relatively low radioactivity. The comparison of the results from this work to the others work will be made afterwards.

2.1   Austenitic Alloy 800H

The proposed advanced nuclear energy systems are aimed to make revolutionary improvements in economics, safety and reliability, and sustainability. To achieve these goals, the reactors will be operated at higher temperatures and to higher accumulated radiation damage than current light water reactors. Metallic alloy components will experience unprecedented microstructural and mechanical property evolution as they progress to higher doses. Of the candidate alloy systems that could be considered for high temperature application, alloy 800H is expected to play an important role as a structural material since it is code certified for temperatures up to 760°C for use in nuclear systems.[1] Alloy 800H has a composition of 31.6 wt.% nickel and 20.4 wt.% chromium. It is expected to exhibit low swelling based on its high Ni content (>30 wt.%), which has been shown in austenitic steels to improve resistance to swelling under neutron irradiation at 400°C to a dose of 18.5 dpa.[2] The alloy also is expected to have good corrosion resistance based on its high Cr content. It is worth mentioning that, among the 4 alloys investigated, both alloy 800H and MA 754 are not the primary candidates for GNEP fuel cladding, although these alloys are capable of operating at high temperature. This is partly due to the high Ni content in these alloys that produces helium through transmutation reaction: $^{58}Ni(n,\gamma)^{59}Ni(n,\alpha)^{56}Fe$.

The alloy 800H used in this work is a commercial grade received in the plate form from Rolled Alloys, Inc. in USA. The material was used in the as-received condition with the final heat treatment at 1,177°C for 2.25 hours followed by a water quench. The unirradiated microstructure of alloy 800H is shown in Figure 1. There were a few large and scattered Ti rich particles (~0.5 μm with ~94 at%Ti and ~3 at%Cr) in the matrix. The alloy has a dislocation density of approximately 4×10^{13} m^{-2}, which is relatively high for the condition of heat-treated at 1,177°C for 2.25 hours.

For the samples irradiated at 500°C to 1.3 dpa in the ATR, the irradiation resulted in significant changes in the microstructure due to the irradiation-induced precipitation (see Figure 2). Two types of precipitates formed, and both crystals have a fixed orientation relationship to the matrix of 800H. One is identified as $M_{23}C_6$, the commonly observed Cr-rich carbide with a fcc crystal structure, uniformly distributed through the grains with many of them showing facet features. The $M_{23}C_6$ precipitates populated at the grain boundaries are larger in size and irregular in shape as shown in Figure 2(a). The insert of the diffraction pattern in Figure 2(c) indicates that the faceted surfaces of $M_{23}C_6$ carbides have {111} type planes with most carbides elongated close to the <220> direction.

The second type of irradiation-induced precipitates, shown as weak contrast, circular features in Figure 2(b), are barely visible in the matrix under bright field image condition. While the dislocation arrangement remains similar between the unirradiated and the irradiated condition, a low density of micro voids (<5 nm) are present in the irradiated sample with a few voids attached to the $M_{23}C_6$ carbides, shown in Figure 2(c). Both the bright field and the rel-rod weak beam dark field images did not reveal any faulted loops in the 800H irradiated at 500°C to 1.3 dpa. A comparison of the selected-area diffraction (SAD) from zone [112] is shown in Figure 3. While the diffraction spots from $M_{23}C_6$ are clearly visible with a 1/3 spacing to the 800H matrix spots, the circle-marked weak spots due to the γ' precipitates are quite faint. Figure 4 shows EDS spectra of the 800H matrix, large Ti rich particles in both unirradiated and irradiated conditions, and the $M_{23}C_6$ Cr rich precipitates in the irradiated condition. The EDS spectrum for γ' could not be characterized due to their small size and the limitations of the electron beam probe size and detector. The composition of γ' is expected to be $Ni_3(Ti, Al)$ with a fcc crystal structure.[3] The γ' precipitates are much better revealed under the weak beam dark field imaging condition using one of the weak spots from γ'; see Figure 5 (top). The irradiated 800H also contains scattered thin platelets, shown in Figure 5 (bottom).

The measurement of micro voids is summarized in Figure 6. Average void diameter, number density, and the corresponding volume swelling are estimated to be 3.6 nm, 2.5×10^{14} cm^{-3} and 7.7×10^{-4} %, respectively. The effect of voids on mechanical property and dimensional stability for alloy 800H irradiated at 500°C to 1.3 dpa is negligible.

For the alloy 800H irradiated at 800°C to 1.5 dpa, the SAD diffractions from zone [112] and [111] are shown in Figure 7. The weak spots due to γ' precipitates are marked with small circles. The diffraction from zone [112] on the left is similar to that of Figure 3. The diffraction of zone [111] shows an enhanced spot intensity from γ' precipitates. The effect of irradiation temperature on the $M_{23}C_6$ precipitates is demonstrated in Figure 8. While Cr carbides in the matrix remain similar in size and distribution, the large Cr carbides at grain boundaries are bigger for irradiation at 800°C than that of 500°C. The lower number of Cr carbides shown in the 800°C irradiation temperature is due to the thinner foil thickness compared to the area imaged for 500°C condition. The measurements on $M_{23}C_6$ Cr carbides in the matrix for both irradiation temperatures are summarized in Figure 9. There is no noticeable change in carbide size, size distribution, and number density between the two irradiation temperatures. The sizes and densities of $M_{23}C_6$ Cr carbides in alloy 800H for the 500°C and 800°C irradiations are estimated to be 34 nm and 35 nm, 5.5×10^{14} cm^{-3} and 5.8×10^{14} cm^{-3}, respectively.

Weak beam dark field images of γ' precipitates in the alloy irradiated at 800°C is shown in Figure 10 with comparison to the irradiation condition at 500°C. There is a dramatic change due to temperature effect on the development of radiation-induced γ' precipitates in alloy 800H. The measurements of the γ' precipitates are summarized in Figure 11. The size distribution is significantly different between the two irradiation temperatures. The comparison of γ' precipitates in alloy 800H irradiated at 800°C vs. 500°C shows a higher number density (1.3×10^{16} cm^{-3} vs. 3.4×10^{14} cm^{-3}), smaller size (12.0 nm vs. 34.7 nm), and higher volume fraction (1.4% vs. 0.9%). The impact of γ' precipitates on the mechanical property of alloy 800H is expected to be larger for the irradiation at 800°C.

2.2   Austentic ODS Alloy MA754

The austenitic ODS alloy MA754 used in this work was received from Special Metals Corporation in the plate form in the recrystallized condition. It is an ODS Ni-based (78%Ni) Ni-Cr super-alloy for high temperature application with excellent high temperature strength and resistance to creep and corrosion. It has a much better oxidation resistance than alloy 800H. According to the alloy specification and technical notes, it is an attractive material to be used for gas turbine engine components, furnace fixtures and fasteners due to its high melting point (1,400°C) and microstructural stability.[4] The stability of oxide dispersions under neutron irradiation is the subject of this work.

The weak beam dark field image using rel-rod imaging technique did not reveal any faulted dislocation loops in the irradiated MA754. No voids are found in this material. Figure 12 shows the dislocation arrangement (top) and oxide particles (bottom) for the unirradiated (left) and the irradiated (right) (500°C, 1.2 dpa) MA754. The images on the top were recorded with diffraction of g={200} to show the dislocation contrast in fcc metal. The dislocation density is quite low in the unirradiated condition. For the sample irradiated at 500°C to 1.2 dpa, the dislocation density is further reduced. The bottom micrographs were imaged without dislocation contrast to show oxide particles. There is no significant change on the oxide particles.

The size distribution, mean particle size, particle volume and number density of oxide particles are summarized in Figure 13. The size distribution remains similar between the unirradiated and the irradiated conditions, with the average particle size of 15 nm vs. 16 nm, and number density of 4×10^{15} cm^{-3} vs. 3×10^{15} cm^{-3}, respectively. Since oxide dispersion particles in MA754 play an important role on its mechanical properties, irradiation at 500°C to 1.2 dpa is expected to have little impact on its mechanical properties.

There are precipitates other than yttrium oxide particles also present in both the unirradiated and the irradiated conditions. Figure 14 shows an area containing the major types of precipitates in MA754. The representative EDS spectra for those precipitates marked in the picture are included in the figure. There are four types of precipitates identified: oxide dispersion particles (compound of Y, Al and O), Ti rich particles, Cr rich particles, and Al rich particles (likely Al oxides). The effect of irradiation on these particles other than yttrium oxide particles could not be quantified due to their low densities and small sizes. Based on their low densities, the impact of these particles on the mechanical properties of MA754 is expected to be insignificant in comparison to the yttrium oxide dispersion particles.

2.3   Ferritic ODS Alloy MA957

MA957 is a ferritic ODS alloy developed for fast reactor cladding application. The mechanically alloyed powders are consolidated by hot extrusion in an evacuated steel can to form wrought bar. The cladding tubes can be made from the bars after a series of steps. The details on the alloy development can be found in reference [5]. The scale of alloy development never reached mass production for commercial use. Major drawbacks of MA957 is its anisotropic grain and subgrain structure and mechanical properties. Another potential limitation in advanced nuclear systems is due to the large amount of Al in the alloy that leads to the formation of alumina stringers believed to be detrimental to the material strength. Recognizing these shortcomings, it was included in this study as a representative ODS alloy developed specifically for nuclear reactor application in the USA.

Alloy MA957 has a messy and complex microstructure with submicron grains, high density of dislocations, subgrain cell structures, and various types of precipitates in addition to yttrium oxide particles. The focus in this work is to investigate the stability of yttrium oxides under neutron irradiation. Composition analysis with EDS for the unirradiated sample revealed both Al rich precipitates and Ti rich precipitates at low densities. EDS measurements for the irradiated samples were not available due to the high background counts from the sample radioactivity. The low magnification TEM images of the general microstructural features are shown in Figure 15 for the conditions of unirradiated (top), irradiated at 500°C to 1.2 dpa (middle), and irradiated at 800°C to 1.4 dpa (bottom). The general microstructural features for all three conditions are dominated by the subgrain cell structures and dislocations. No significant changes can be identified. Since all the TEM disc samples are made with its surface normal aligned to the rolling direction of the bar, all the grains or subgrains appear equal-axial.

High magnification TEM images showing dislocation arrangement among the three conditions are shown in Figure 16. The dislocation configurations appear to remain similar for the unirradiated and the irradiated at 500°C and 800°C to 1.2~1.4 dpa. No dislocation loops were found in the irradiated samples. Radiation-induced voids were not present. There is no noticeable annealing effect on the dislocations arrangement for the 800°C irradiation. Yttrium oxide dispersion particles are believed to play an important role in stabilizing the dislocation configuration in the irradiated MA957.

Radiation effects on yttrium oxide particles are shown in Figure 17. For the unirradiated condition, the distribution of yttrium oxide particles, particularly the large particles, is relatively non-uniform. Two images are shown at the top for the unirradiated condition with one from an area mainly consisting of small spots (~2 nm) and the other one from an area containing clusters of large particles. The irradiation at 500°C to 1.2 dpa seemingly eliminated the clusters of large yttrium particles with more pronounced development of the small particles. The irradiation at 800 to 1.4 dpa reveals only few scattered large yttrium particles with matrix mostly decorated with small yttrium particles. From the EDS measurement, most of the large particles shown in Figure 17 contain Y, Ti, Al, and O. The measurements of size distribution, average size, and number densities for yttrium oxide dispersion particles for the three conditions are summarized in Figure 18. The change in particle size distribution clearly illustrates the reduction of large yttrium particles and promotion of the small particles for irradiation at 500°C and 800°C to 1.3 dpa. The sizes of yttrium oxide particles for the unirradiated, irradiated at 500°C and at 800°C are 10 nm, 7 nm and 6 nm, respectively. The corresponding number densities of the oxide dispersion particles are 1.8×10^{15} cm^{-3}, 3.1×10^{15} cm^{-3}, and 5.6×10^{15} cm^{-3}, respectively. The trend appears that irradiation at 500°C/1.2 dpa and 800°C/1.4 dpa tends to slightly shrink the particle size and increase the particle density in MA957.

2.4 Ferritic Alloy HCM12A

HCM12A is an advanced 12 Cr ferritic alloy developed for high temperature application. It has been considered for application in core components in Generation IV nuclear energy system as well as for advanced cladding materials in the GNEP program due to its anticipated excellent resistance to corrosion and void swelling. Note that the 12Cr alloy HT9 was the most advanced cladding and duct material used in the fast reactors of the Fast Flux Test Facility (FFTF) and Experimental Breeder Reactor (EBR)-II.[6] HCM12A is designed to operate at an upper temperature limit (~620°C) approximately 55°C higher than HT9.[7]

HCM12A used in this work was obtained in plate form from Sumitomo Metal Industries, Kashima Steel Works in Japan. The alloy was normalized at 1,050°C followed by air-cooling and then tempered at 770°C followed by air-cooling. The average grain size of the prior austenite grains is 14±3 μm. The general microstructures for both the unirradiated and the irradiated HCM12A are shown in Figure 19. Most of the precipitates present are identified as $M_{23}C_6$ carbides. The population of carbides at grain boundaries in the irradiated (500° and 1.1 dpa) sample is higher than the unirradiated condition. The overall microstructure for both conditions is dominated by the dense dislocations and carbides. A close-up look at the irradiated microstructure is shown in Figure 20. The image on the top shows the dislocation network and a few scattered dislocation loops along with precipitates, while the image at the bottom shows the spot feature uniformly distributed in the matrix. Since black dot damage is expected to occur only at relatively low irradiation temperature (<300°C for stainless steel),[8] these spot features may have been introduced during TEM sample preparation by the radiation damage from room temperature ion milling or the initial stage of small precipitates.

Small voids were found with relatively high density in the irradiated HCM12A in only one area of approximately ~10 μm^2; see Figure 21. This represents less than 1% of the total thin area examined. It was a surprise, since voids are not expected in this material at ~1 dpa. No voids are found in the other part of the irradiated sample. The chemical analysis and the crystal structure analysis for the area with voids revealed no noticeable difference to the rest of the sample. The cause of void development in this particular area is not clear. Both local chemical fluctuation and residual austenite grain in this particular area in the unirradiated sample may be responsible for the void development. Note that void swelling peaks around irradiation temperature of 550°C for the austenitic stainless steel. Void distribution and measurement of this 10 μm^2 area are summarized in Figure 22. The average void size, number density, and corresponding swelling are 2.7±0.9 nm, 4.3×10^{16} cm^{-3} and 0.06%, respectively.

3.   DISCUSSIONS

The results of the TEM microstructutal analysis for the four advanced alloys irradiated with neutrons in ATR at irradiation temperatures of ~500°C and ~800°C to doses of 1.1~1.4 dpa have been presented in the previous sections. This section will discuss those results in comparison with the relevant irradiation work of others. Both neutron irradiation and ion irradiation will be included. The discussion will provide some insights into the feasibility of these alloys to be used for cladding or other core components.

3.1   Alloy 800H

The dramatic change in the 800H microstructure irradiated to relatively low dose (~1 dpa) is expected to significantly degrade the alloy performance. Radiation hardening from precipitates is expected to be large even without faulted loops. Note that, at 500°C irradiation, large faulted loops are a signature feature of radiation damage in the microstructure of austenitic alloys. The lack of faulted loops at 500°C irradiation is likely due to the development of both types of precipitates ($M_{23}C_6$ and γ'). These precipitates serve as neutral sinks for point defects; therefore, the amount of interstitials available for nucleation and growth of faulted loops are significantly reduced. The accumulation of large Cr-rich $M_{23}C_6$ at grain boundaries from irradiation could alter the grain boundary chemistry by Cr depletion and weaken the grain boundaries. The impact of small voids at low density in the matrix should have no effect on the material performance at dose up to 1.3 dpa. The thin platelets shown in Figure 5 (image at bottom) are likely stacking faults. These features are narrower than typical stacking faults in 304 SS, possibly due to the higher Ni content in 800H associated with a higher stacking fault energy. The impact of these stacking faults on the mechanical properties of the irradiated 800H is expected to be less important due to their low density.

The Ni ion irradiation of 800H at 500°C to 5 dpa revealed faulted loops with size and density of 13 nm and 1.2×10^{16} cm^{-3}, respectively.[9] No voids were found even for doses up to 50 dpa. Radiation-induced precipitates were identified only in the 50 dpa condition with size and density of 6 nm and 9.1×10^{15} cm^{-3}, respectively. The chemical analysis for these small precipitates was not successful due to their small size. Considering the high damage rate in Ni ion irradiation, the 500°C irradiation temperature simulates the neutron irradiation condition around 350°C. The lack of $M_{23}C_6$ and γ' in the Ni ion irradiated 800H is likely due to the effect of temperature shift. The lack of He production from transmutation of Ni in Ni ion irradiation may explain the absence of voids in the Ni ion irradiation study of alloy 800H. The different irradiated microstructure of 800H observed in neutron-irradiated and Ni ion-irradiated at 500°C material indicates that the use of Ni ion irradiation to simulate neutron irradiation consider should consider the effects of the high damage rate on sample temperature and microstructure development.

Gelles, et al. conducted an irradiation study on a very similar alloy (Alloy 800) irradiated with neutrons in EBR-II at 425°C and 540°C to ~100 dpa, and the alloy developed severe void swelling to 41% and 12%, respectively. Small and finely distributed MC precipitates and large γ' precipitates were present. No $M_{23}C_6$ type precipitates were reported in the irradiated alloy 800. The γ' precipitates after 540°C irradiation are much larger than after 425°C irradiation. The difference between Gelles' work and this work is mostly due to the large difference in dose in addition to the irradiation temperature difference.

At 800°C irradiation, there is a strong temperature effect on the precipitates. The Cr carbide precipitates at grain boundaries are larger than that observed in the 500°C irradiation. The most noticeable change is γ' precipitates, with significantly smaller size and higher density at 800°C irradiation. At this irradiation temperature, both faulted loops and voids are not expected to be present. Nucleation of γ' precipitates is enhanced at 800°C irradiation. The smaller size is likely due to the limited amount of Al and Ti available for the growth of γ' in high density. The radiation hardening from both $M_{23}C_6$ and γ'can be estimated using the dispersion barrier hardening model for changes in yield strength:[10]

$$\Delta\sigma_y = 3.06\alpha\mu b\sqrt{N \cdot d}$$

where α is the barrier strength factor (~1 for precipitates), μ is the shear modulus, b is the Burgers vector for network dislocation, N is the number density, and d is the size of precipitates. For austenitic alloys, μ=76GPa and b=2.55×10^{-8} cm. The calculated precipitate contribution to the radiation hardening is listed in Table 3. It is clear that the irradiation hardening due to γ' at 500ºC irradiation is similar to that caused by carbides. For irradiation at 800°C, radiation hardening significantly increases and is dominated by γ' precipitates. Radiation hardening is detrimental to the material performance in irradiation environment. The severe radiation hardening of alloy 800H at relatively low irradiation dose suggests that this material should not be used as cladding or other core components exposed to neutron irradiation in the service temperature of 500-800°C.

Table 3. Estimate of precipitate contributions to irradiation hardening in alloy 800H.

Precipitates type	Irradiation temperature (ºC)	Irradiation dose (dpa)	Precipitate density (10^{15} cm^{-3})	Precipitate size (nm)	Hardening $\Delta\sigma_y$ (MPa)
γ'	500	1.3	0.34	34	202
γ'	800	1.5	13	12	741
Carbide	500	1.3	0.55	34	256
Carbide	800	1.5	0.58	35	267

3.2   Austentic ODS Alloy MA754

There is a paucity of microstructural data in the open literature for neutron-irradiated MA754. The lack of research interest in this area for MA754 is probably due to it being a Ni-base alloy, which alloy class generally exhibits poor void swelling resistance under neutron irradiation due to helium production. Nickel transmutes to helium, and the helium production rate is proportional to the Ni content.[11] The alloy used in this work was in the recrystallized condition with a very low dislocation density. The lack of voids and faulted loops in MA754 irradiated at 500°C to 1.2 dpa in this work is possibly attributed to the oxide dispersion particles promoting point defect recombination at the interface of the dispersion particles and the matrix. Low dislocation density also makes void development more difficult due to the lack of biases sinks for preferential absorption of interstitials at dislocations. Irradiation to 1.2 dpa slightly increases the average particle size and decreases particle density; however, these small changes are statistically insignificant. The material performance is expected to be the same between the unirradiated and the irradiated at 500°C to 1.2 dpa.

Shirashi et al. in their work reported that voids were nucleated preferably on the oxide-matrix interface for the helium pre-injected (~300 appm) MA754 irradiated with protons at 450-600°C to 20 dpa.[12] It was found that swelling increases with irradiation temperature to approximately 1%, 3%, 5%, and 10% at 450, 500, 550, and 600°C, respectively. The anticipated swelling reduction by oxide dispersion particles was not observed in their work. It suggests that the oxide dispersion particles in austenitic ODS alloys are not effective in suppressing void swelling. The major differences between their work and this work are on the irradiation dose (20 dpa vs. 1.2 dpa) and irradiation type (proton with He pre-injection vs. neutron). It is anticipated that MA754 may develop void swelling at higher dose due to its high Ni content providing a source of helium production. The future work on the high dose irradiation of MA754 will be necessary to confirm this hypothesis.

3.3   Ferritic ODS Alloy MA957

The microstructure of ferritic ODS MA957 is very different than the austenitic ODS MA754. Dislocation density is very high and the grain size is very small in MA957. The stability of the dislocation microstructure in the irradiated MA957 is evident as shown in Figures 15-16. The lack of changes for irradiation at both 500°C and 800°C is likely due to the combined effects of the high density of dislocations, subgrain boundaries and oxide dispersion particles. A high density of oxide dispersion particles stabilizes the dislocation arrangement and subgrain boundaries even at irradiation temperature of 800°C, which impedes thermal recovery and prohibits grain growth. Note that dislocation bias for bcc is lower than fcc. The retention of a very high dislocation density maintains a strong sink for both interstitials and vacancies, which effectively limits the development of irradiation-induced defect microstructure. Other important facts for the bcc crystal include high self-diffusion, low helium generation rate (<1% Ni) and high subgrain boundaries sink strength, making the alloy inherently more swelling resistant than fcc austenitic alloys.[13]

The irradiation at 500°C and 800°C to 1.2-1.4 dpa did not significantly affect the oxide dispersion particles. There is no evidence of any coarsening of oxide particles; see Figure 17. In contrast to a coarsening effect on the oxide dispersion particles, the irradiation eliminated the clusters of large yttrium oxide particles and enhanced the number density of small oxide particles in the irradiated MA957 with average oxide particle sizes of 10 nm, 6.9 nm and 6.0 nm for the unirradiated, irradiated at 500°C to 1.2 dpa and irradiated at 800°C to 1.4 dpa, respectively. This trend is consistent with the heavy ion irradiation study of a 9Cr ferritic ODS alloy.[14] The small reduction in size and increase in number density for oxide dispersion particles are believed to be beneficial to the alloy performance under irradiation.

Gelles et al. reported that no microstructural evidence was found in MA957 for radiation damage after irradiation at 550°C to a dose of 8.0×10^{22} n/cm^2 (40 dpa) [5]. The mechanical tests performed by Gelles et al. showed no difference in yield strength between the unirradiated and the irradiated at 500° and 700°C to 28.5 dpa. The irradiation at 750°C to 40 dpa revealed a microstructure similar to that of 550°C except the presence of clusters of small cavities within the large TiO_2 precipitates. No quantitative measurement was conducted on the radiation stability of oxide dispersion particles. Their results, regardless the large difference in irradiation doses to this work, are consistent with the results in this work with irradiation at 500°C and 800°C to 1.2 and 1.4 dpa, respectively. The large difference in the irradiated microstructure between the high dose irradiations of MA754 (proton, 20 dpa) and MA957 (neutron, 40 dpa) reported in the open literature suggests that the role of oxide dispersion particles on swelling resistance is less important than the crystal structure (fcc vs bcc), the original dislocation arrangement, and the grain structure (low dislocation density vs. high dislocation and subgrain densities). The importance of the oxide dispersion particles on materials performance is due to its effect on high temperature mechanical strength. The role of oxide particles on the radiation resistance is believed to be secondary through the mechanism of stabilizing the dislocation and subgrain microstructure.

3.4   Ferritic Alloy HCM12A

Alloy HCM12A has an initial microstructure typical of ferritic stainless steels with precipitates in different size and shapes distributed in the matrix and at the grain boundaries. These precipitates are mostly identified as $M_{23}C_6$ carbides. The only visible change from irradiation at 500°C to 1.1 dpa is the slightly increased precipitate population at the grain boundaries and the presence of a few scattered dislocation loops. The presence of voids at this relatively low dose in one area of the sample is quite surprising; see Figure 21. These voids are still in the incubation stage since the average diameter of mature voids should be much larger at the irradiation temperature of 500°C. Since the rest of the TEM sample analyzed is free of voids and the area fraction showing voids is very small (<1%), micro voids should not be considered a representative defect feature in HCM12A irradiated at 500°C to 1.1 dpa.

The Ni ion irradiation of the same alloy at 500°C to 5 and 50 dpa revealed no changes in microstructure at 5 dpa and few scattered dislocation loops in areas with a high density of dislocations at 50 dpa.[15] The dominant microstructural features for both unirradiated and the Ni ion-irradiated HCM12A are dense dislocations with $M_{23}C_6$ precipitates. No voids were found even at 50 dpa. The proton irradiation of the same alloy at 400ºC to 10 dpa revealed voids (6.2 nm size, 9.4×10^{14} cm^{-3} density, 0.015% swelling), small precipitates (5.7 nm size, 3.9×10^{15} cm^{-3} density), and dislocation loops (34 nm size, 3.2×10^{14} cm^{-3} density, $a_0<100>$ type). The composition and crystal structure information of the small precipitates could not be obtained due to their small size and detector limit. For comparison with previous neutron irradiation data, HT-9 (12Cr-1MoVW) is considered a similar ferritic alloy to HCM12A with excellent swelling resistance. After irradiation in FFTF to 35 and 205 dpa at 420°C, the void swelling in HT-9 estimated from TEM data was only 0.007% and 0.09%, respectively.[16,17] HCM12A is expected to exhibit similar swelling resistance to HT-9 with an improvement on its upper limit of application temperature. The lack of microstructural change in this work is expected, since the irradiation dose of 1.1 dpa is too low to show any noticeable change.

4.   SUMMARY

The results of TEM analysis of the four advanced alloys, 800H, MA754, MA957 and HCM12A, have been presented. These materials are all developed for high temperature applications. The microstructural analysis of these alloys irradiated in ATR at 500 and 800ºC to doses of 1.1-1.5 dpa lead to the following conclusions. Alloy 800H experienced the most significant changes in the microstructure, dominated by irradiation induced precipitates. The irradiation induced precipitation (and projected hardening) is much worse at 800°C than at 500°C. The significant microstructural changes material should not be considered to be used in irradiation environments at high temperature, particularly at 800°C. No significant changes are identified in both ODS alloys, MA754 and MA957, on the irradiated microstructure. The oxide dispersion particles remain stable under the irradiation conditions investigated. Austenitic ODS alloy MA754 is anticipated to develop void swelling due to its high Ni content, therefore it should not be considered for high irradiation field application. Two ferritic alloys, ODS MA957 and HCM12A, showed no significant changes in the irradiated microstructure. Both are good candidate materials to be used for GNEP cladding program. However, ferritic ODS alloy should only be considered if an upper temperature limit higher than that for HCM12A (~620°C) becomes necessary. The future work on the high dose (>10 dpa) irradiation of the same set of alloys will provide valuable information to a better understanding of the microstructural performance under neutron irradiation.
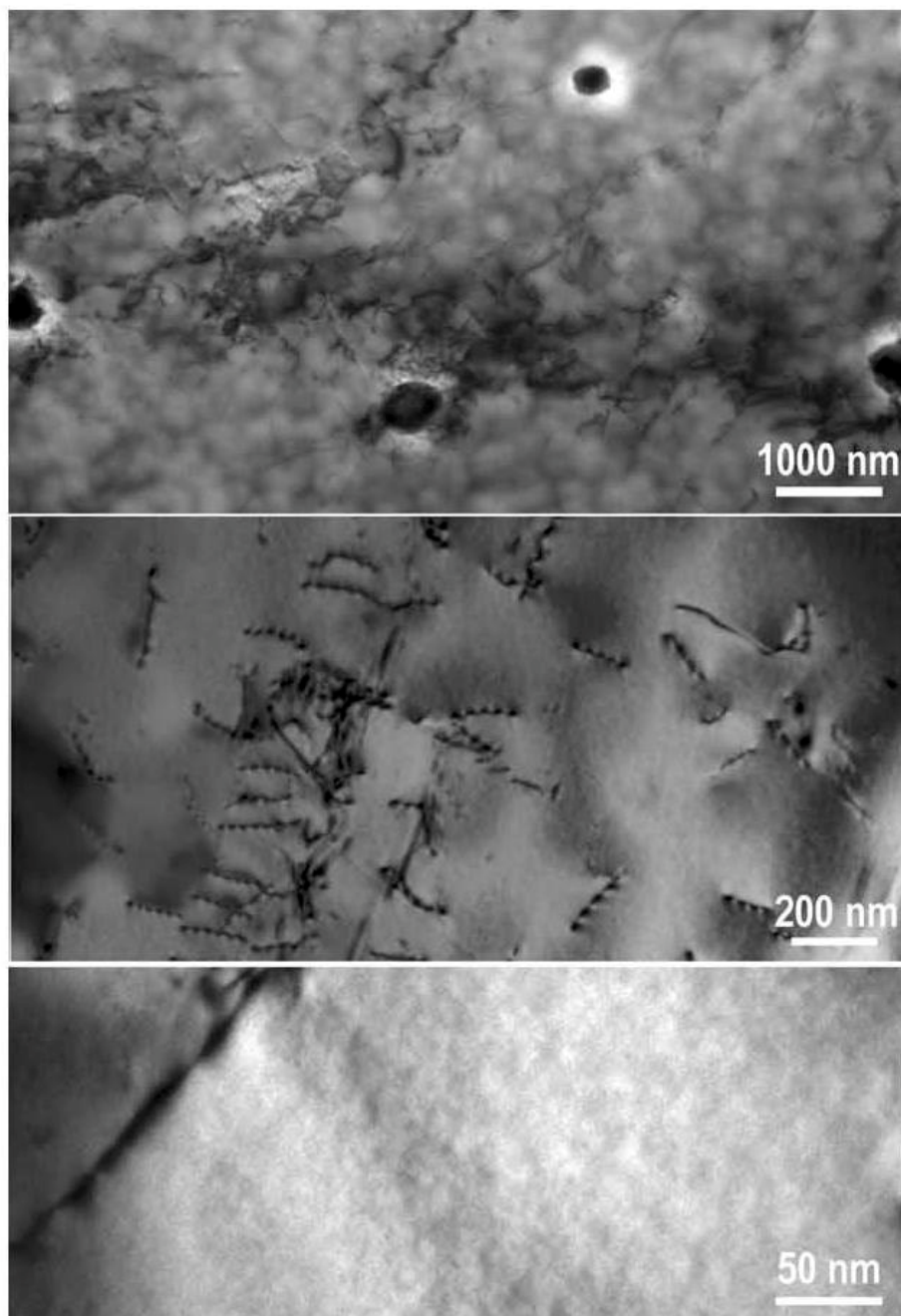
Figure 1. Unirradiated microstructure of alloy 800H (imaged with g=200 diffraction) reveals large and scattered Ti rich particles (top), dislocations in low magnification (middle), and high magnification (bottom).
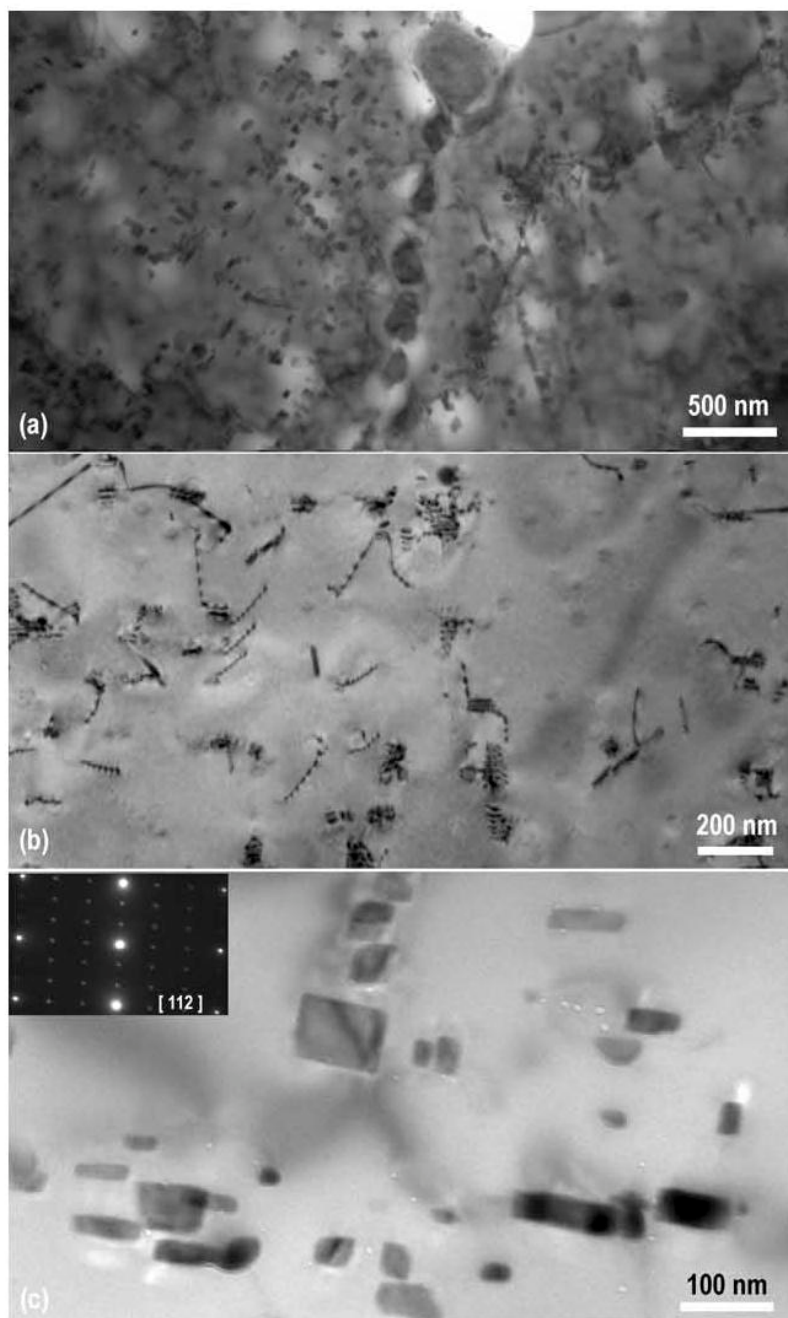
Figure 2. Bright field images showing defect features in the alloy 800H irradiated with neutrons at 500°C to 1.3 dpa. (a) distribution of $M_{23}C_6$ precipitates with small ones in the matrix and the large ones at the grain boundaries, (b) dislocations and the circular γ' precipitates in the weak contrast, and (c) the high magnification view of the faceted feature of $M_{23}C_6$ precipitates and micro voids (<5 nm) in the white contrast.
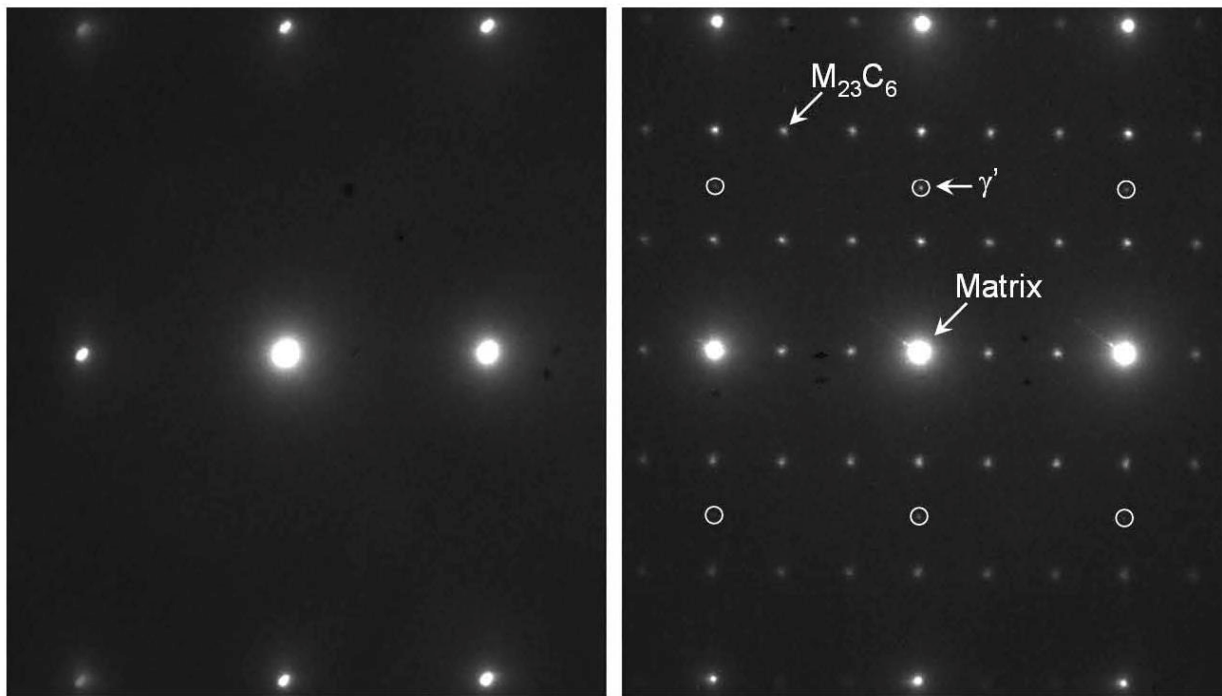
Figure 3. Comparison of <112> zone diffraction in alloy 800H between the unirradiated (left) and the neutron-irradiated at 500°C to 1.3 dpa (right). Two types of coherent precipitates are found in the irradiated alloy, and the circles mark the weak spots due to γ' precipitates.
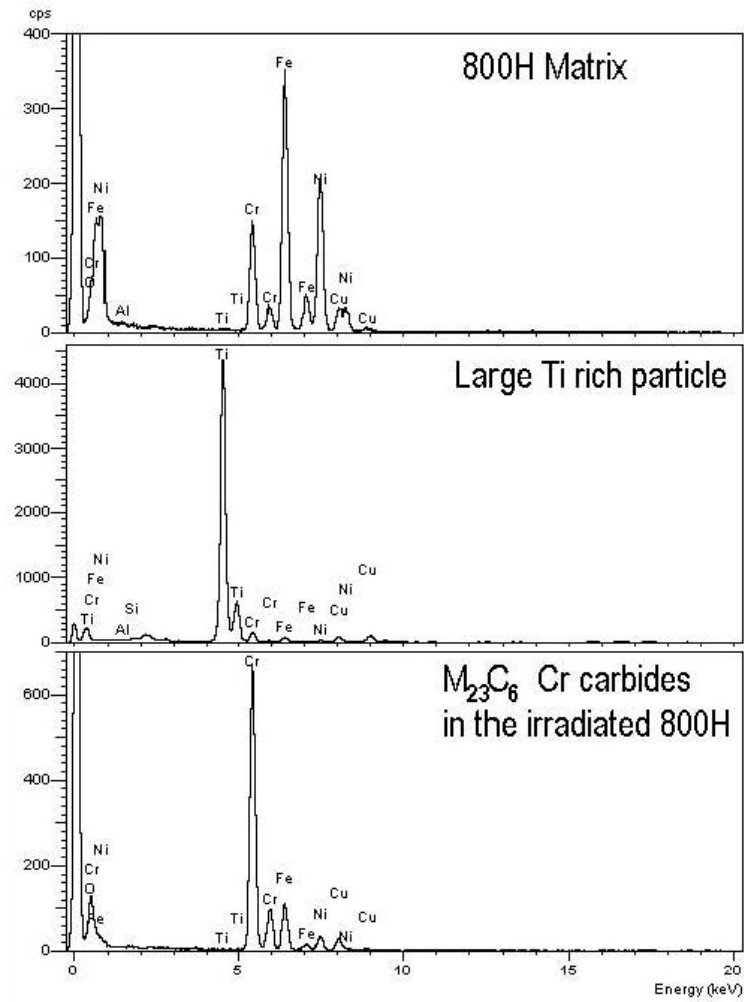
Figure 4. EDS plots of alloy 800H for the matrix (top), the large Ti-rich particles existed in both the unirradiated and the irradiated condition (middle), and the $M_{23}C_6$ precipitates in the irradiated condition (bottom). EDS measurement of irradiation-induced γ' precipitates is not quantifiable due to their small size.
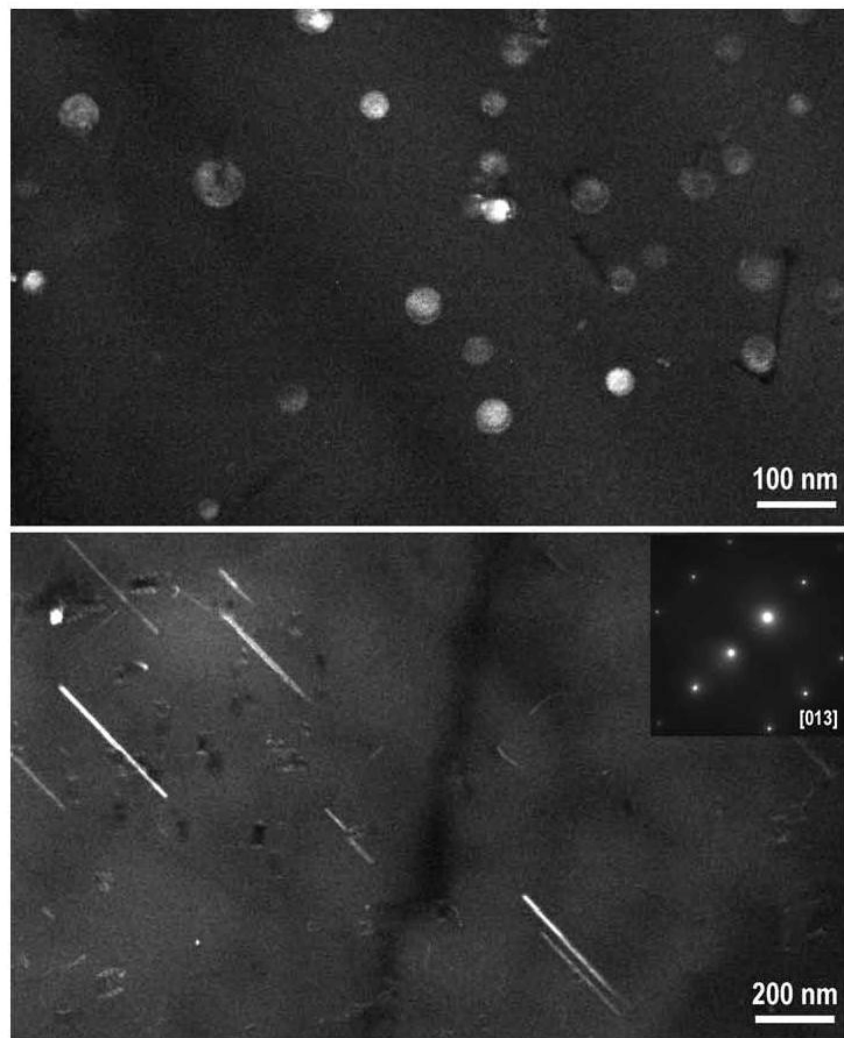
Figure 5. Weak beam dark field images showing the circular γ' precipitates (top) and the thin plate features (bottom) in the alloy 800H irradiated with neutrons at 500°C to 1.3 dpa.
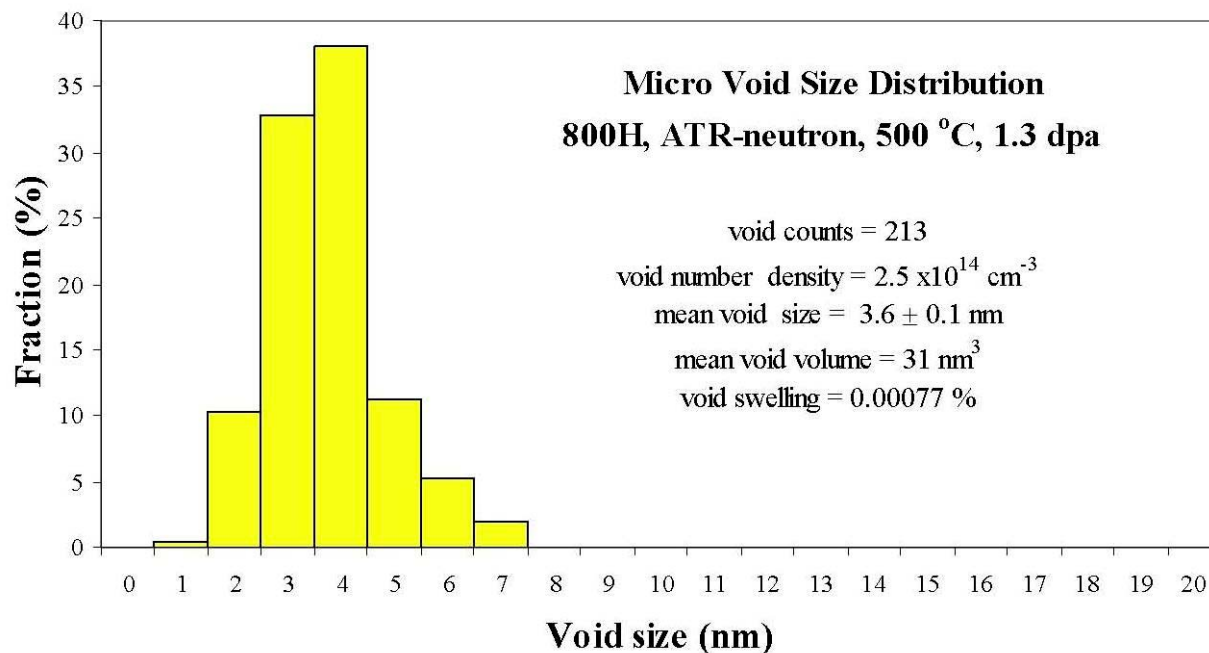
Figure 6. Size distribution of micro voids in the alloy 800H irradiated at 500°C to 1.3 dpa. Note that the corresponding swelling and hardening are expected to be negligible.
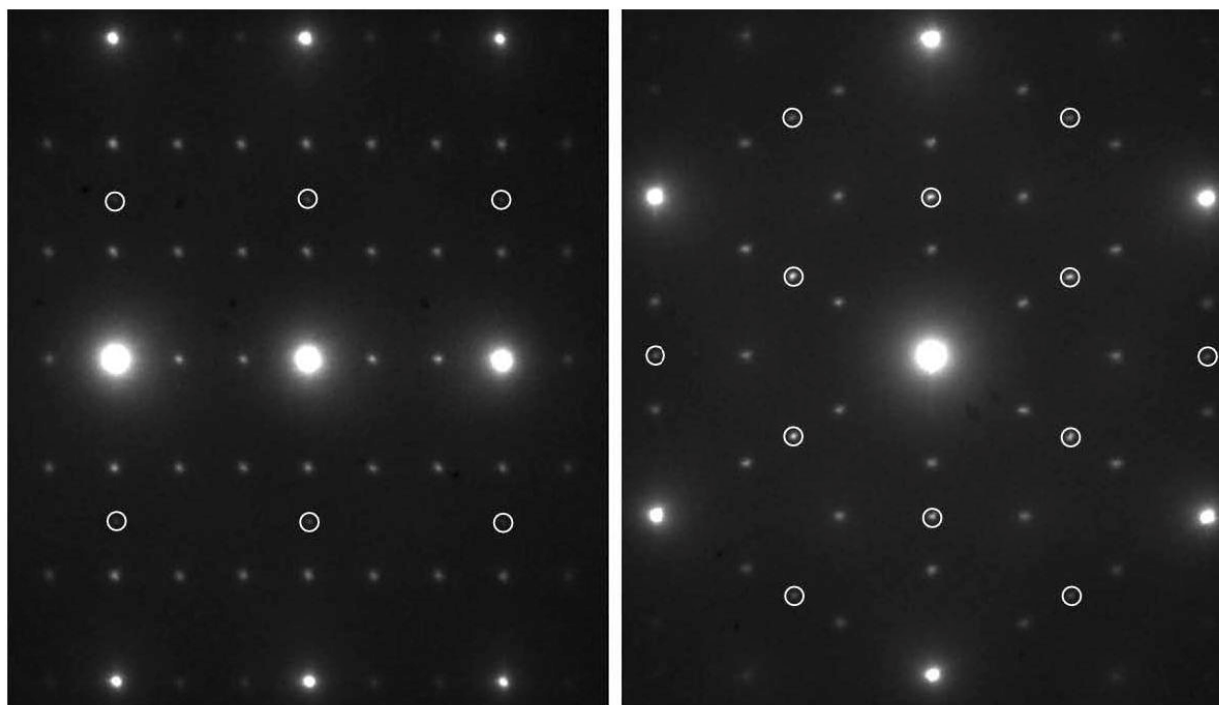
Figure 7. Selected area diffractions of zone <112> (left) and zone <111> (right) for alloy 800H irradiated with neutrons at 800°C to 1.5 dpa. There are two types of coherent precipitates found in the irradiated alloy; the circles mark the weak spots due to γ' precipitates, while the rest of the weak spots are due to $M_{23}C_6$ precipitates.
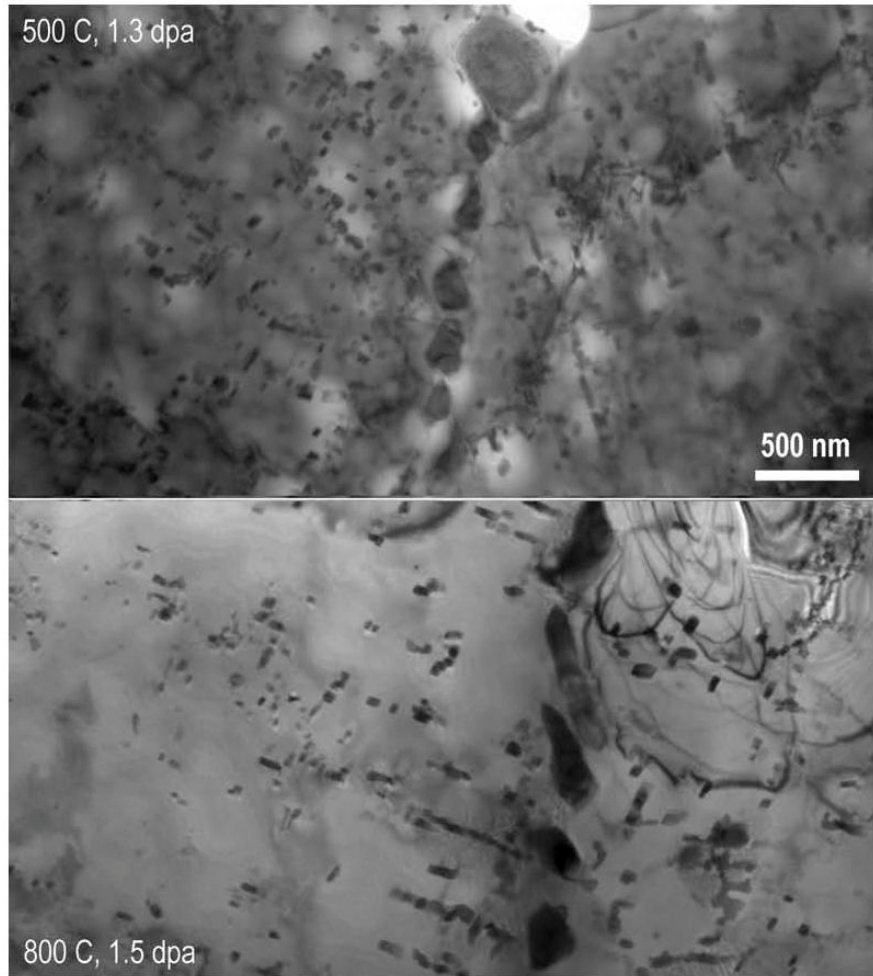
Figure 8. Bright field images showing comparison of irradiation-induced $M_{23}C_6$ precipitates in the alloy 800H irradiated with neutrons at 500°C to 1.3 dpa (top) and 800°C to 1.5 dpa (bottom). Note that the precipitates at the grain boundaries are larger for the irradiation at 800°C.
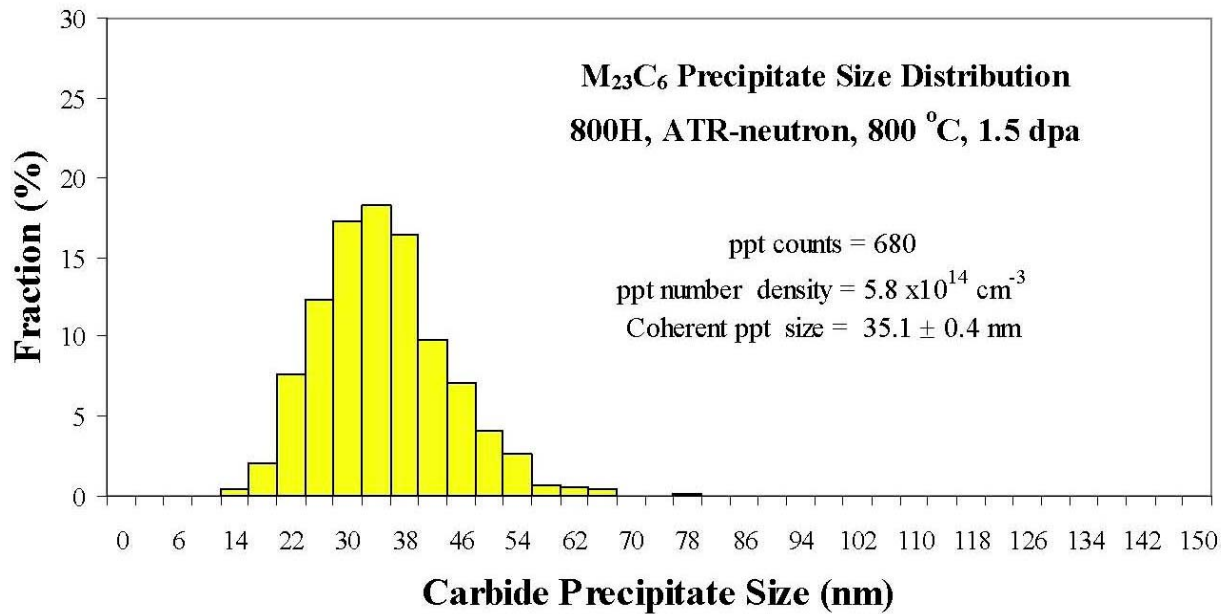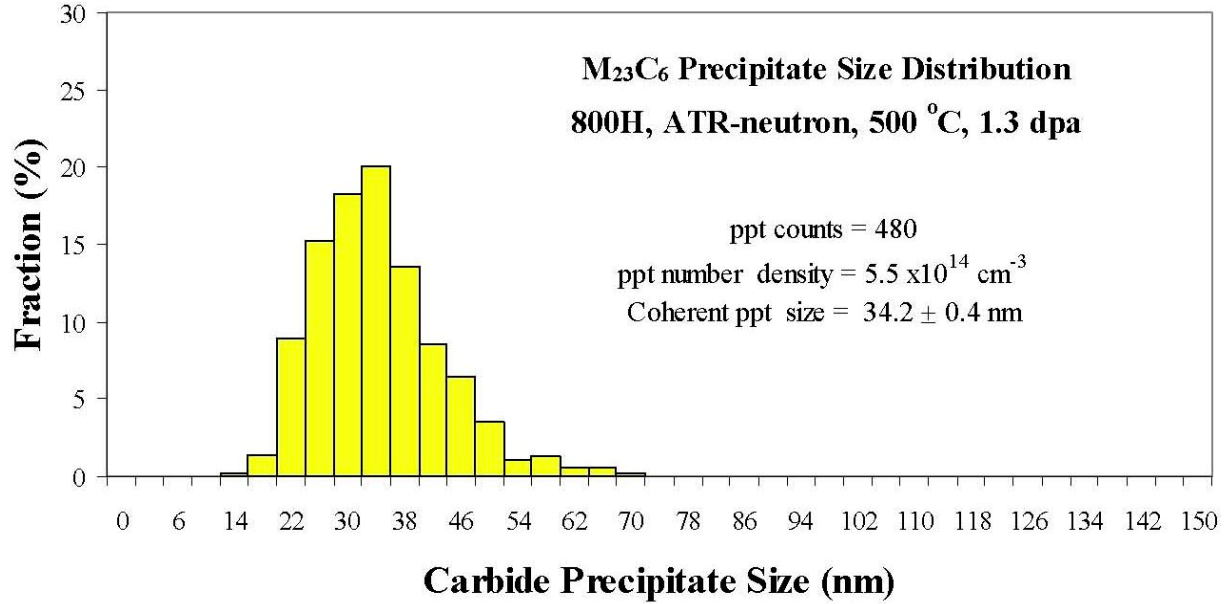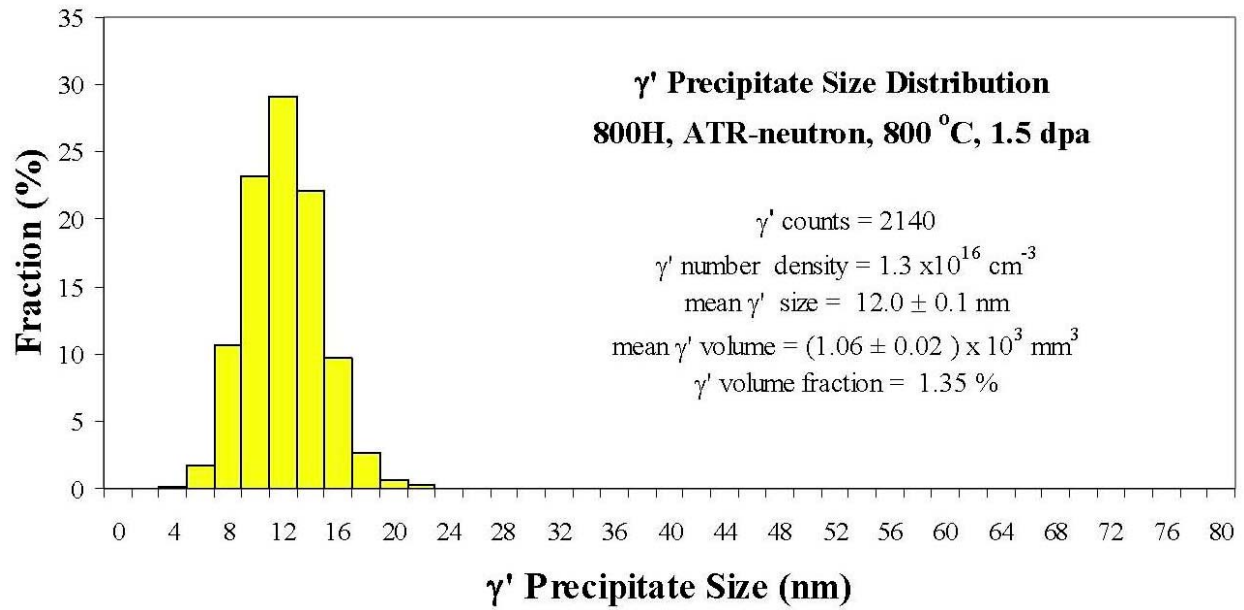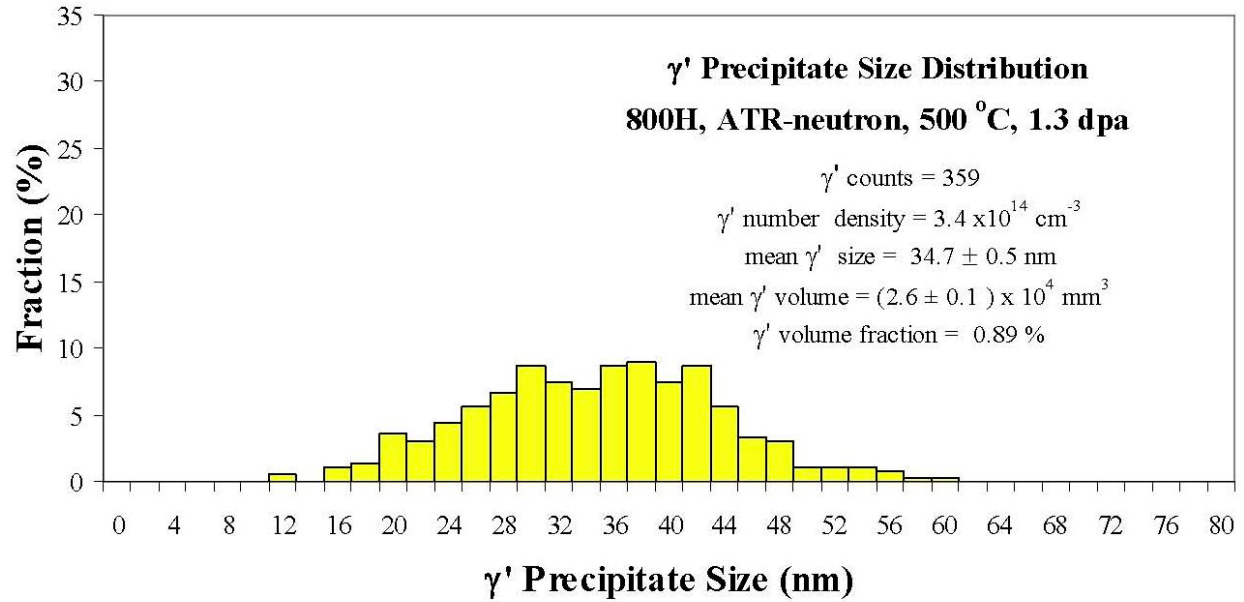
Figure 9. Comparison of size distributions for the irradiation-induced $M_{23}C_6$ precipitates in the alloy 800H irradiated with neutrons at 500°C to 1.3 dpa (top) and 800°C to 1.5 dpa (bottom). There is no significant change on $M_{23}C_6$ precipitates between the two irradiation conditions.
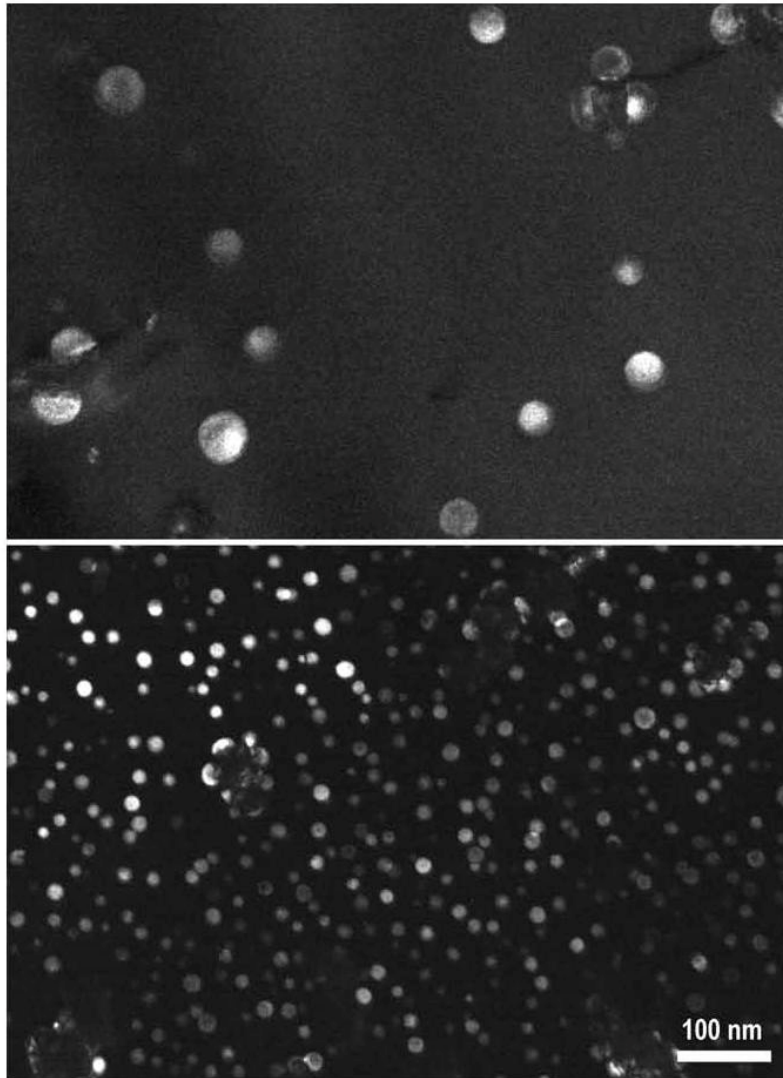
Figure 10. Weak beam dark field images comparing irradiation-induced γ' precipitates in the alloy 800H irradiated with neutrons at 500°C to 1.3 dpa (top) and 800°C to 1.5 dpa (bottom).

Figure 11. Comparison of size distributions for the irradiation-induced γ' precipitates in the alloy 800H irradiated with neutrons at 500°C to 1.3 dpa (top) and 800°C to 1.5 dpa (bottom). There is a significant change on the size and number density of γ' precipitates.
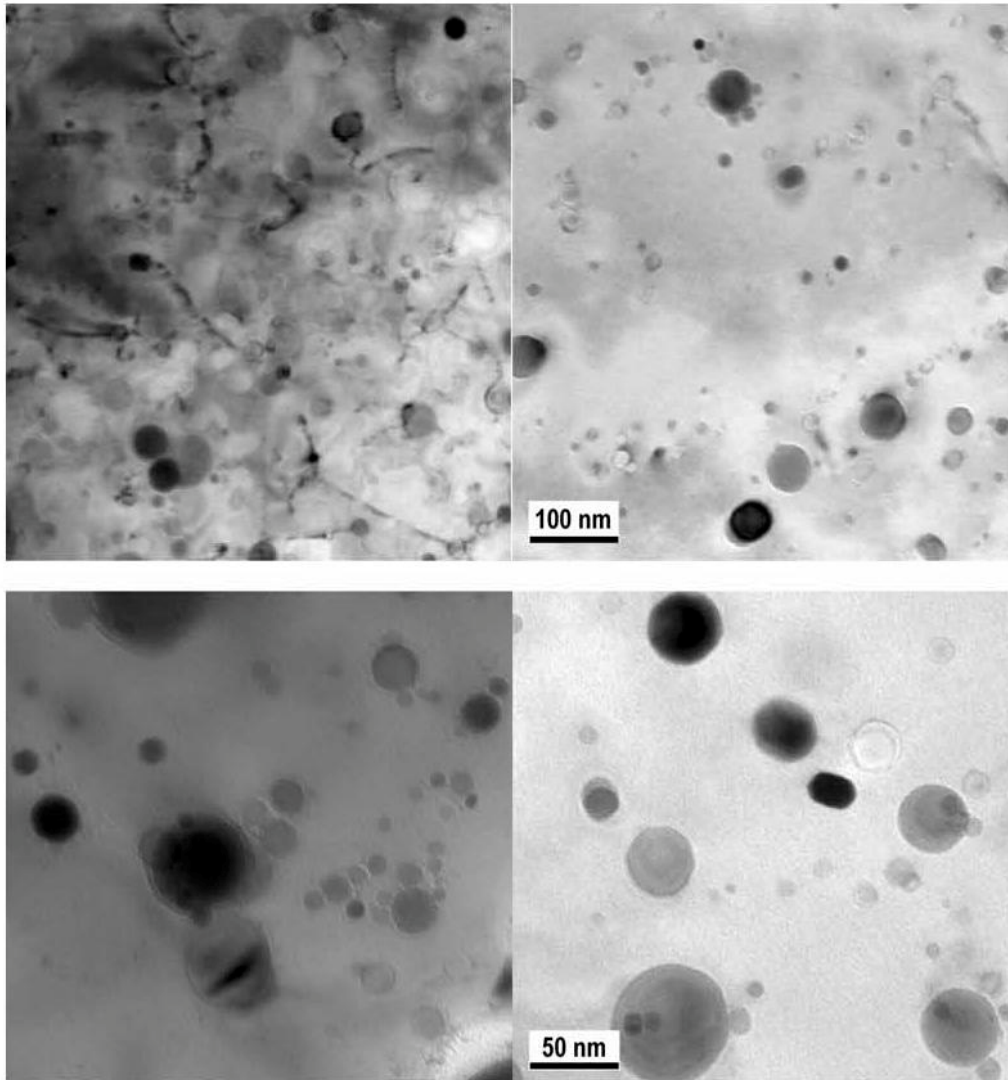
Figure 12. Yttrium oxide particles in alloy MA754 for the unirradiated (left) and the irradiated with neutrons at 500°C to 1.2 dpa (right). The images on the top show dislocation contrast using g=200, and the images on the bottom show irradiation effect on yttrium oxides. Dislocation density in the irradiated MA754 is significantly lower, while the irradiation effect on yttrium oxide is not significant.
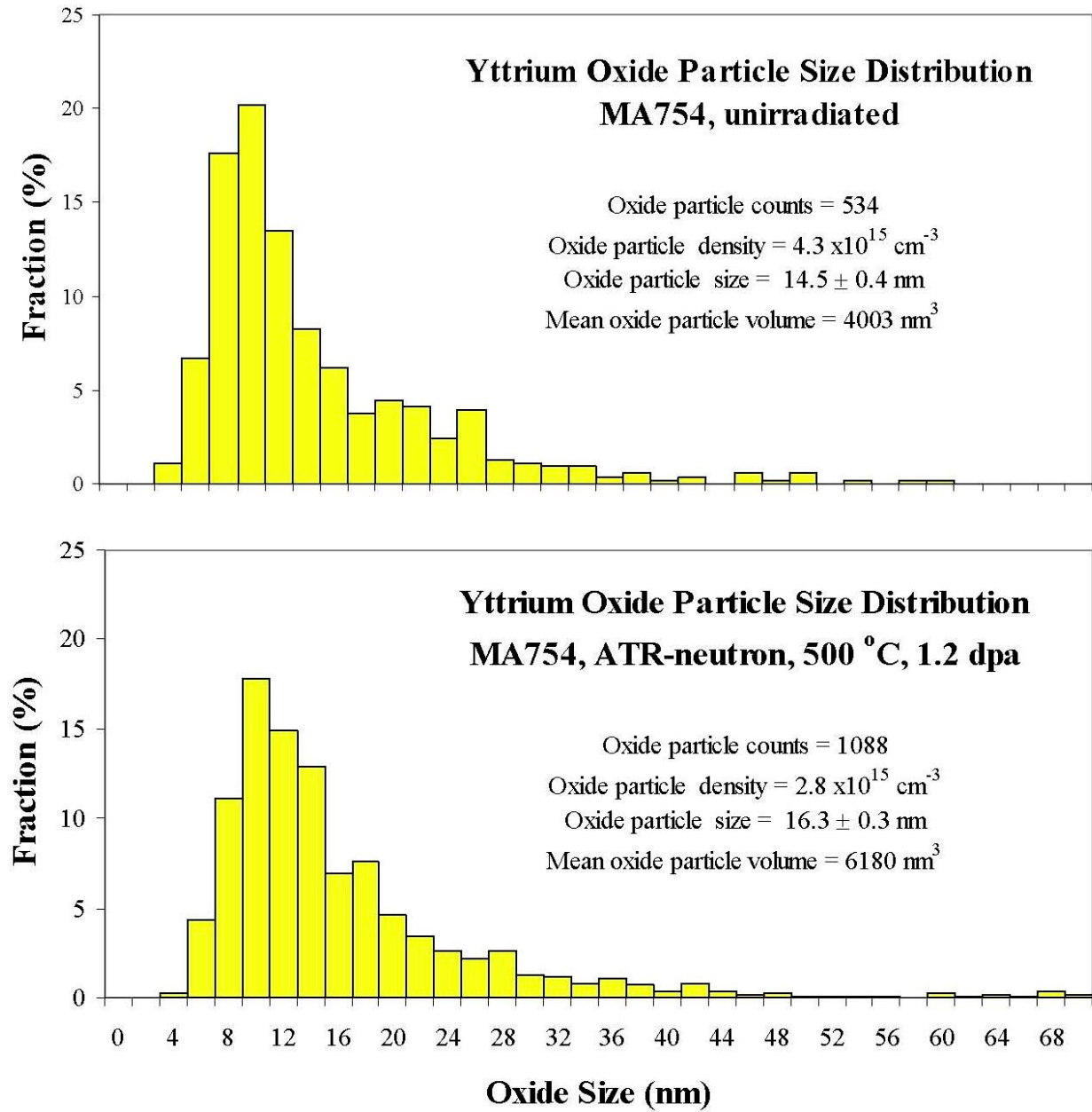
Figure 13. Size distribution of yttrium oxide particles in alloy MA754 for the unirradiated (top) and the irradiated with neutrons at 500°C to 1.2 dpa (bottom). There is no significant change in average size, size distribution, and number density of the oxide particles.
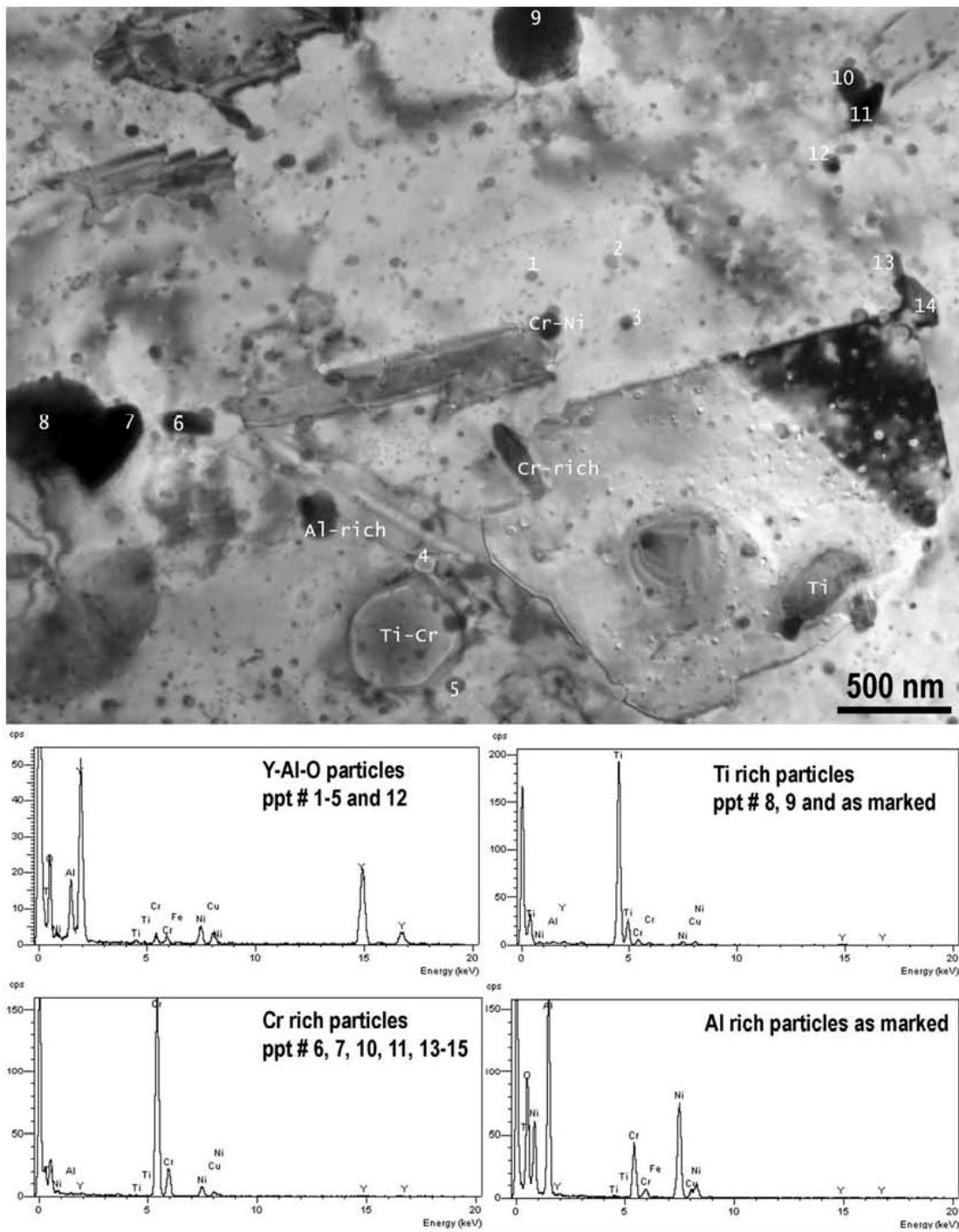
Figure 14. Various precipitates found in both the unirradiated and the irradiated alloy MA754 (at 500°C to 1.2 dpa). The plots show the EDS measurement for the major precipitates identified in the alloy.
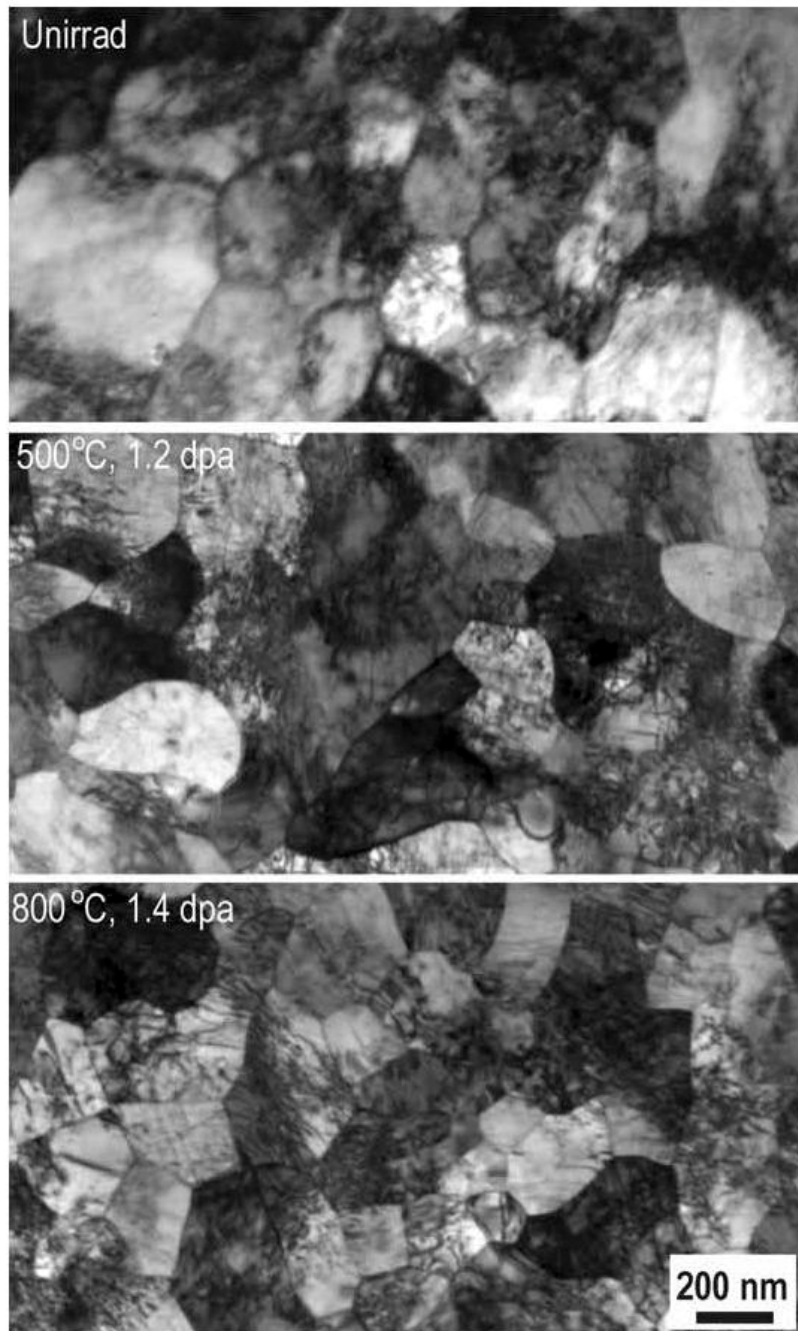
23

Figure 15. Low magnification images of microstructural features in MA957 for the unirradiated (top), the irradiated at 500°C to 1.2 dpa (middle), and at 800°C to 1.4 dpa (bottom). No noticeable changes in the general microstructure.
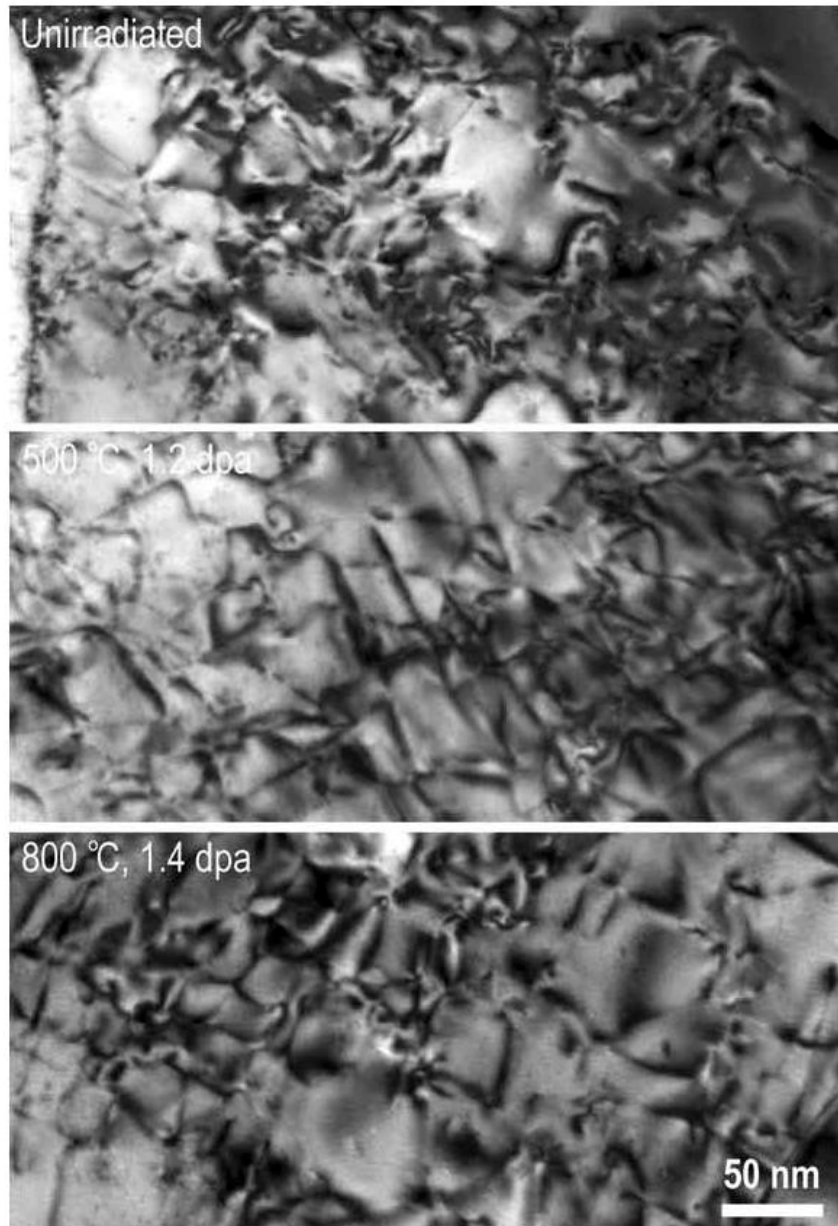
Figure 16. High magnification images of dislocations in MA957 for the unirradiated (top), the irradiated at 500°C to 1.2 dpa (middle), and at 800°C to 1.4 dpa (bottom). No noticeable changes in the dislocation configuration.
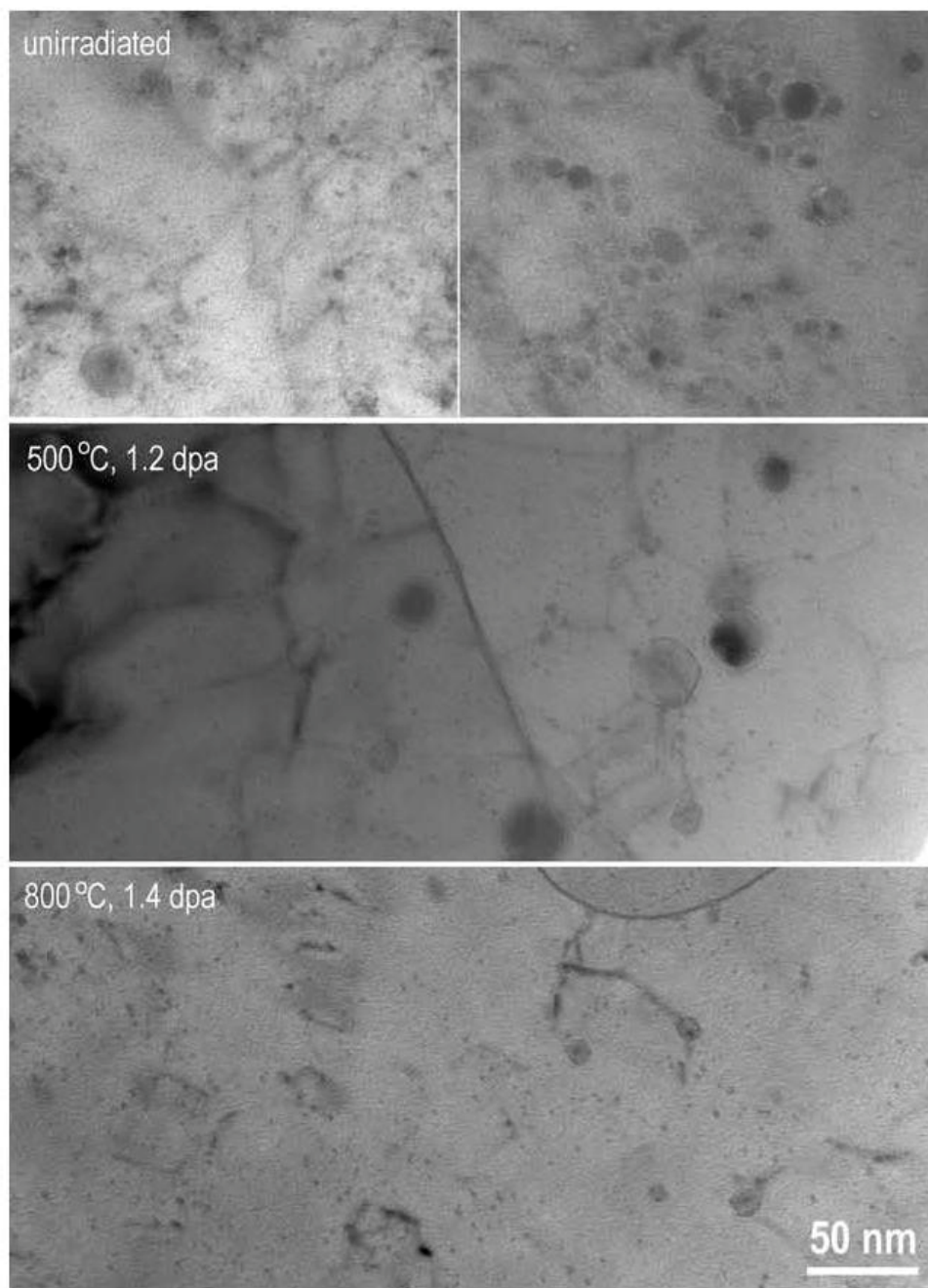
Figure 17. High magnification images of yttrium oxide particles (large circular features and small spots) in MA957 for the unirradiated (top), the irradiated at 500°C to 1.2 dpa (middle), and at 800°C to 1.4 dpa (bottom).
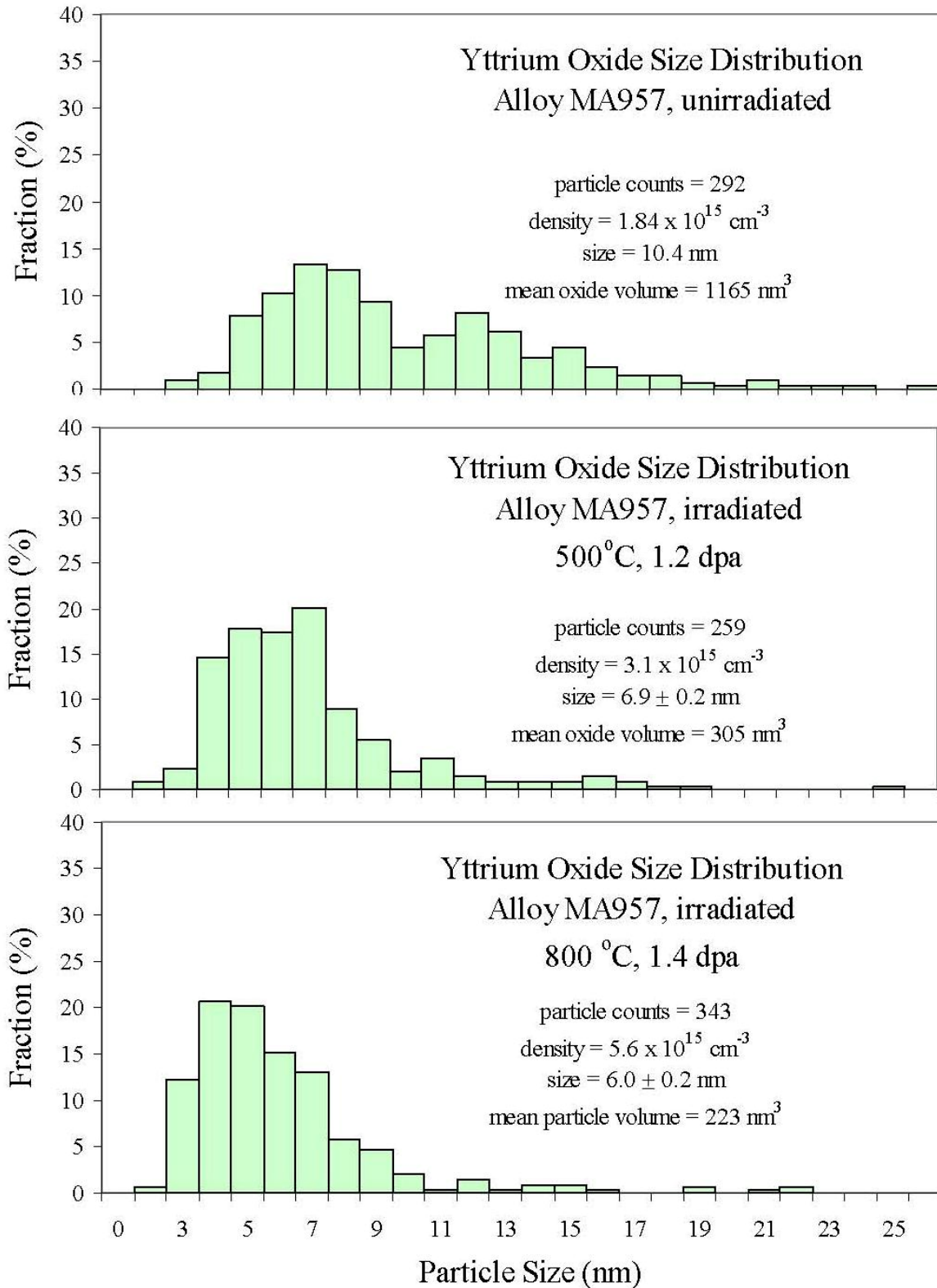
Figure 18. Size distribution of yttrium oxide particles in MA957 for the unirradiated (top), the irradiated at 500°C to 1.2 dpa (middle), and at 800°C to 1.4 dpa (bottom). Irradiation resulted in smaller average sizes and higher densities of the oxide particles.
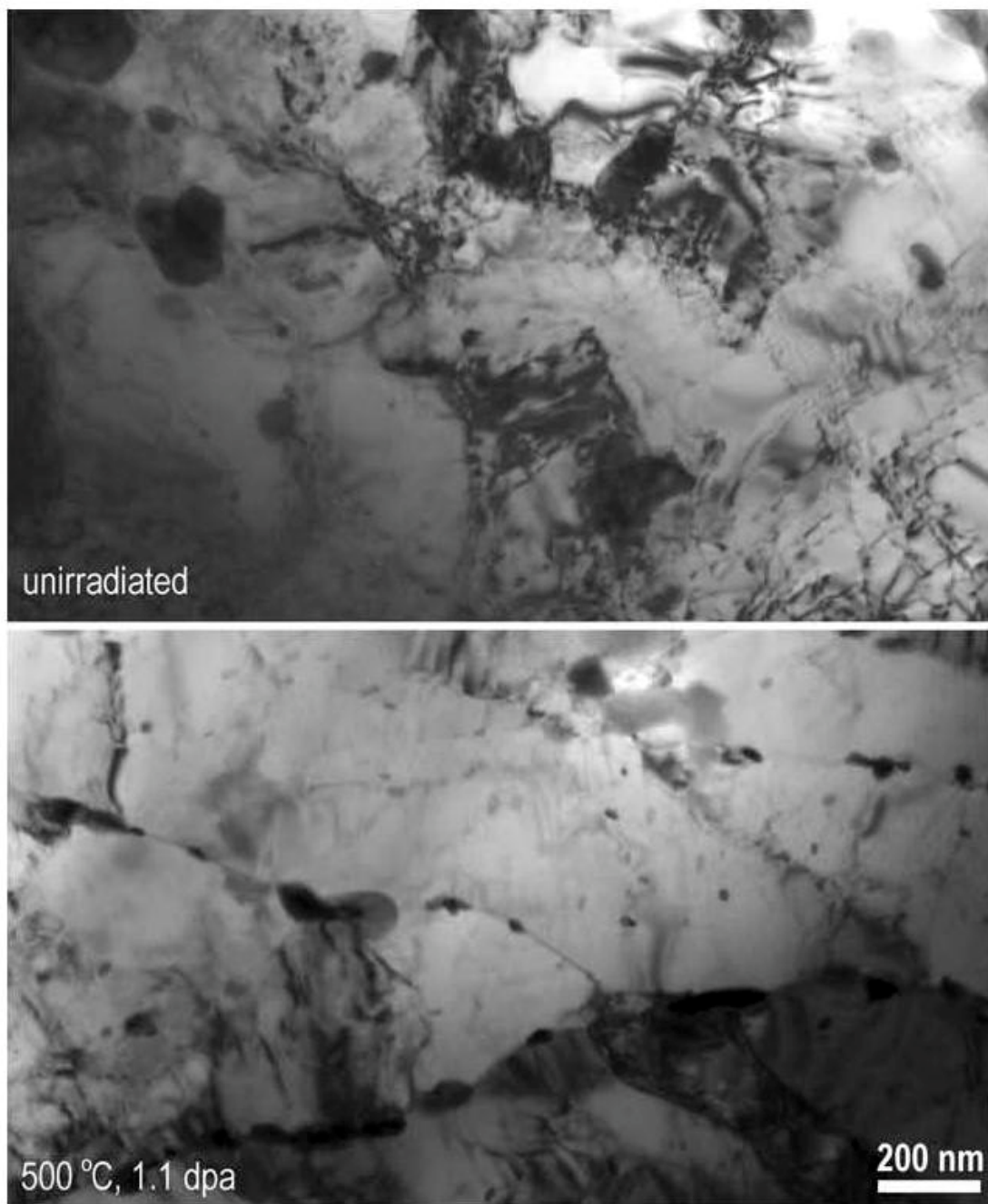
Figure 19. Low magnification images of general microstructural features in HCM12A for the unirradiated (top) and the irradiated at 500°C to 1.1 dpa (bottom).
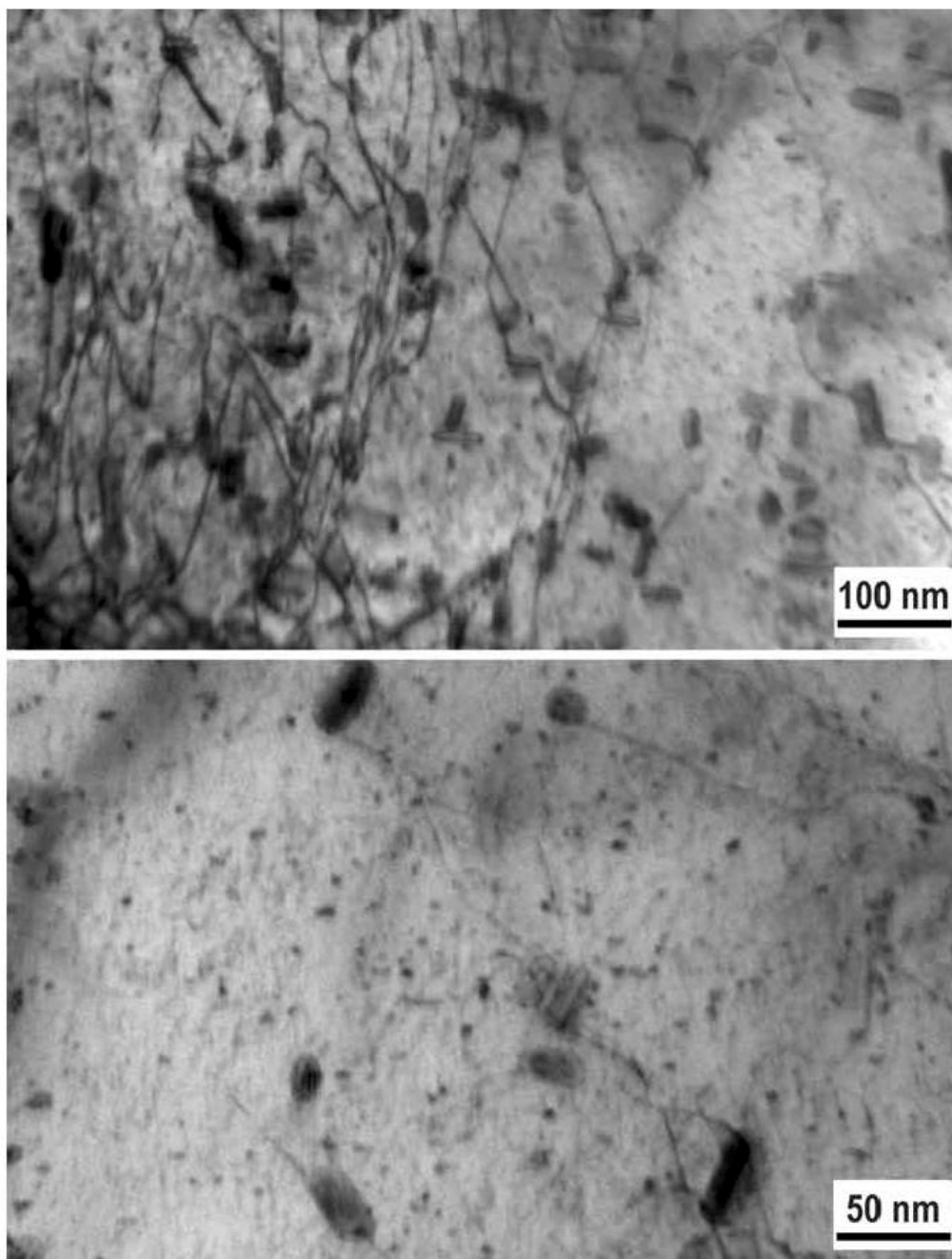
Figure 20. High magnification image showing dislocations (g=1,-1,0), precipitates (top) and black dots in HCM12A irradiated at 500°C to 1.1 dpa (bottom). Few scattered dislocation loops are visible in the image on the top.

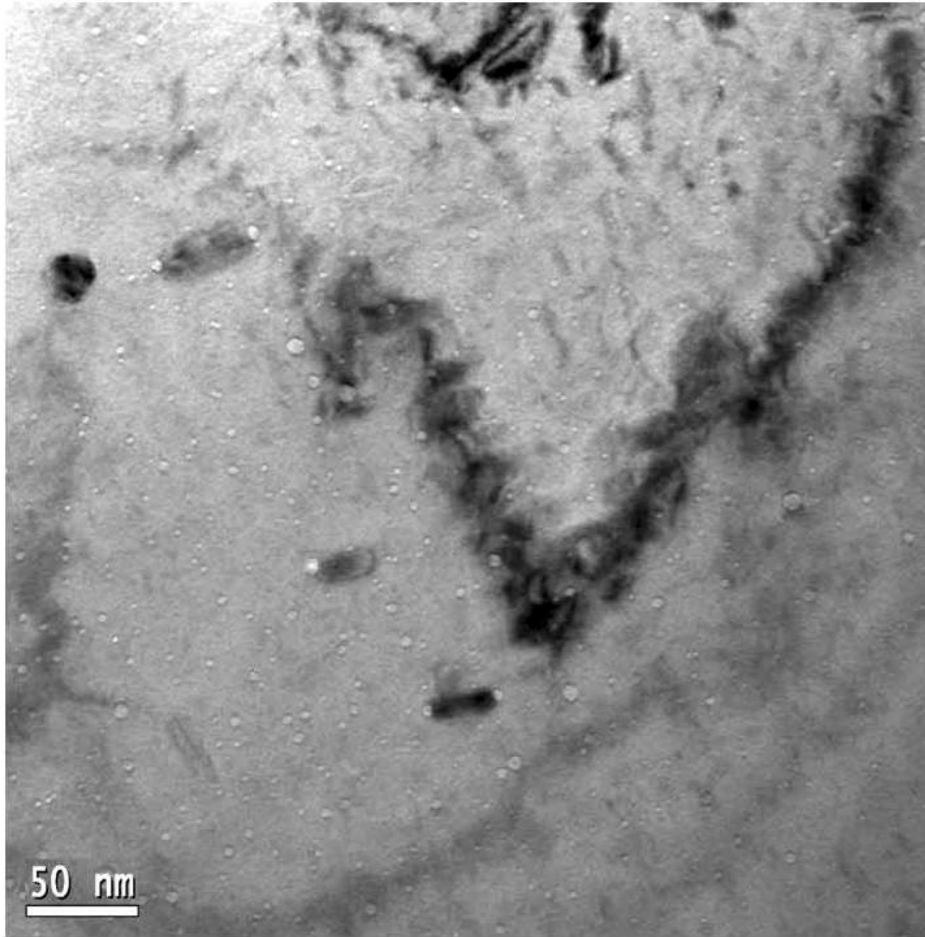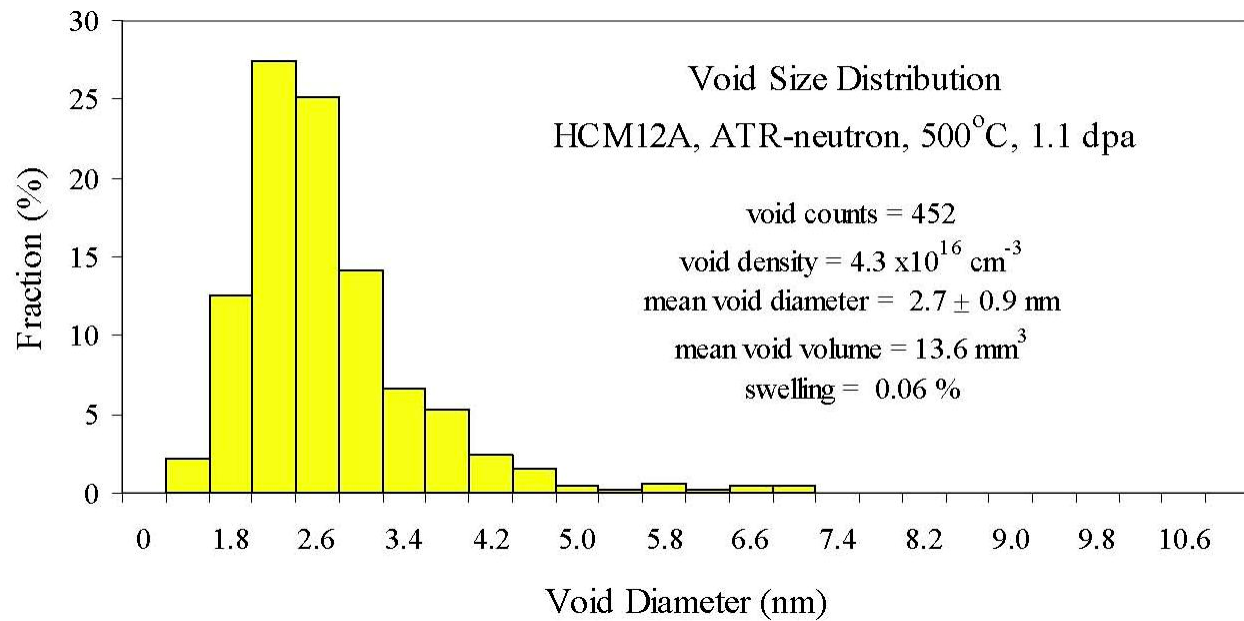Figure 21. Voids are found in one area (~10 μm^2) of the HCM12A alloy irradiated at 500°C to 1.1 dpa.

Figure 22. Summary of measurement for voids found in a particular area (~10 μm^2) of the HCM12A alloy irradiated with neutrons at 500°C to 1.1 dpa.

5. REFERENCES

1. Natesan, K., A. Purohit, S. W. Tam, and C. A. Greene., 2003, "Materials Behavior in HTGR Environments," ANL-02/37 and NUREG/CR-6824.

2. Garner, F. A., and A. S. Kumar, 1987, "Radiation-Induced Changes in Microstructure: 13th International Symposium (Part I)," ASTM STP 955, Eds: F. A, Garner, N. H. Packan, and A.S. Kumar, ASTM, Philadelphia, pg. 289.

3. Harris, D. R., 1981, "Physical Metallurgy of Fe-Cr-Ni austenitic Steels," *Proceedings of the InternationalConference on Mechanical Behavior and Applications of Stainless Steels at Elevated Temperature*; May 1981, Publisher: The Metals Society, London, pg. 1.

4. Technical Notes of MA754 at www.specialmetals.com.

5. Hamilton, M. L., D. S. Gelles, R. J. Lobsinger, G. D. Johnson, W. F. Brown, M. M. Paxton, A. J. Puigh, C. R. Eiholzer, C. Martinez, and M. A. Blotter, "Fabrication Technological Development of the Oxide Dispersion Strengthened Alloy MA957 for Fast Reactor Application," Pacific Northwest National Laboratory, Report No. PNNL-13168.

6. Leggett, R. D., and L. C. Walters, 1993, *Journal of Nuclear Materials*, 204 (1993) 23.

7. Viswanathan, R., and W. T. Bakker, 2000, *Proceedings of the 2000 International Joint Power Generation Conference*, Miami Beach, FL, July, 2000, pg.1.

8. Zinkle, S. J., P. J. Maziasz, and R. E. Stoller, 1993, *Journal of Nuclear Materials*, 206 (1993) 270.

9. Gan, J., J. I. Cole, T. R. Allen, S. Shutthanandan, and S. Thevuthasan, 2006, *Journal of Nuclear Materials*, 351 (2006) 223-227.

10. Lucus, G. E., 1993, *Journal of Nuclear Materials*, 206 (1993) 292.

11. Garner, F. A., 1994, "Irradiation Performance of Cladding and Structural Steels in Liquid Metal Reactors," Vol. 10A, *Materials Science and Technology*, Edited by R. W. Cahn, P. Haasen, and E. J. Kramer (1994), pg. 420.

12. Shiraishi, H., and A. Hasegawa, 1988, *Journal of Nuclear Materials*, 155-157 (1988) 1049-1053.

13. Odette, G. R., 1988, *Journal of Nuclear Materials*, 155-157 (1988) 921-927.

14. Allen, T. R., J. Gan, J. I. Cole, S. Ukai, S. Shutthanandan, and S. Thevuthasan, 2005, "The Stability of 9Cr-ODS Oxide Particles Under Heavy Ion Irradiation," *Nuclear Science and Engineering,* 151 (2005) 305.

15. Allen, T.R., L. Tan, J. Gan, G. Gupta, G. S. Was, E. A. Kenik, S. Shutthanandan, and S. Thevuthasan, 2006, *Journal of Nuclear Materials*, 351(1-3) (2006) 174-186.

16.   Kai, J. J., and R. L. Klueh, 1996, *Journal of Nuclear Materials*, 230 (1996) 116.

17.   Gelles, D.S., and A. Kohyama, DOE Report DOE/ER-031316, pg. 193.